J. Fluid Mech. (2003), *vol.* 492, *pp.* 303–338.
DOI: 10.1017/S0022112003005809 Printed in the United Kingdom

Thermocapillary instability and wave formation on a film falling down a uniformly heated plane

By S. KALLIADASIS[1], E. A. DEMEKHIN[2], C. RUYER-QUIL[3] AND M. G. VELARDE[4]

[1]Department of Chemical Engineering, University of Leeds, Leeds, LS2 9JT, UK

[2]Department of Chemical Engineering, University of Notre Dame, Notre Dame, IN 46556, USA

[3]Laboratoire FAST, UMR CNRS 7608, Université Paris VI et Paris XI, Campus universitaire, 91405 Orsay, France

[4]Instituto Pluridisciplinar, Universidad Complutense, Paseo Juan XXIII, No. 1 28040-Madrid, Spain

(Received 21 August 2002 and in revised form 28 May 2003)

We consider a thin layer of a viscous fluid flowing down a uniformly heated planar wall. The heating generates a temperature distribution on the free surface which in turn induces surface tension gradients. We model this thermocapillary flow by using the Shkadov integral-boundary-layer (IBL) approximation of the Navier–Stokes/energy equations and associated free-surface boundary conditions. Our linear stability analysis of the flat-film solution is in good agreement with the Goussis & Kelly (1991) stability results from the Orr–Sommerfeld eigenvalue problem of the full Navier–Stokes/energy equations. We numerically construct nonlinear solutions of the solitary wave type for the IBL approximation and the Benney-type equation developed by Joo *et al.* (1991) using the usual long-wave approximation. The two approaches give similar solitary wave solutions up to an $O(1)$ Reynolds number above which the solitary wave solution branch obtained by the Joo *et al.* equation is unrealistic, with branch multiplicity and limit points. The IBL approximation on the other hand has no limit points and predicts the existence of solitary waves for all Reynolds numbers. Finally, in the region of small film thicknesses where the Marangoni forces dominate inertia forces, our IBL system reduces to a single equation for the film thickness that contains only one parameter. When this parameter tends to zero, both the solitary wave speed and the maximum amplitude tend to infinity.

1. Introduction

A layer of viscous fluid falling down an inclined uniformly heated plane, is subject to surface and Marangoni instabilities. In their pioneering study of this problem, Goussis & Kelly (1991) performed a linear stability analysis based on Orr–Sommerfeld and linearized energy equations. They provided a detailed numerical solution of the pertinent eigenvalue problem and demonstrated that a heated wall has a destabilizing effect on the free surface while a cooled wall stabilizes the flow. The thermocapillary instability of a horizontal liquid layer heated from below was considered by Goussis & Kelly (1990) while a number of theoretical works have been devoted to the thermocapillary instability in the case of a temperature gradient along the liquid layer (Smith & Davis 1983*a*, *b*).

In this study we consider the problem of a thin liquid film falling down a uniformly heated plane for small and moderate Reynolds numbers (in the region ∼10–30). Particular emphasis is given to the nonlinear regime of the surface-tension-gradient Marangoni-driven instability. Our analysis is based on the integral-boundary-layer (IBL) approximation of the Navier–Stokes/energy equations and free-surface boundary conditions. This approach in the absence of Marangoni effects was introduced by Shkadov (1967, 1968) in two dimensions and by Demekhin & Shkadov (1984) in three dimensions. It combines the boundary-layer approximation of the Navier–Stokes equation assuming a self-similar parabolic velocity profile and long waves on the free surface with the Kármán–Pohlhausen averaging method in boundary-layer theory. This *ad hoc* approach results in a system of three coupled nonlinear partial differential equations for the evolution of the local film height and flow rates in the streamwise and transverse directions respectively. When thermal effects are present, we expect an additional equation for the interface temperature field. The IBL approximation in this case was recenty derived by Kalliadasis, Kiyashko & Demekhin (2003) in their study of the thermocapillary instability of a thin liquid film heated from below by a local heat source.

This derivation is reviewed in § 2. In § 3 we study the linear stability of the trivial solution with respect to three-dimensional disturbances and we show that by increasing the Marangoni number the instability to three-dimensional disturbances becomes stronger. The remainder of the paper focuses on two-dimensional disturbances. We demonstrate that the role of the Marangoni effect is to amplify and increase the instability of the downstream propagating surface mode such that this mode is characterized by an unusually large growth rate for very thin films. This points to the possibility of very interesting behaviour of the nonlinear solutions in this region.

In § 4 we derive reduced models obtained from our Shkadov model in certain regimes of the parameter space. In particular, when the film thickness tends to zero we derive a single equation with only one parameter, δ, and valid for all flow conditions which indicates a *universal* behaviour as a function of δ in the limit of zero film thickness. In § 5 we construct numerically nonlinear solutions of solitary wave type for the full IBL and the IBL with the free-surface temperature field slaved to the film thickness. We find that the difference between the two approaches for the temperature field becomes large in the region of moderate Reynolds numbers where the convective terms of the energy equation are important. On the other hand, the feedback of the temperature field to the film thickness in this region is small, since the Marangoni forces are not important for thick films in comparison with inertia forces. An impressive feature of our solitary wave solution branch for the speed and maximum amplitude of the solitary waves as a function of Reynolds number is that as the Reynolds number approaches zero, the solitary wave solution branch tends to infinity. Finally, we contrast our solitary wave solution branch with the Joo, Davis & Bankoff (1991) model based on the long-wave lubrication approximation.

2. Formulation

We consider a thin liquid film of viscosity μ, surface tension σ and density ρ falling down a uniformly heated planar inclined wall with inclination angle θ with respect to the horizontal direction. Figure 1 sketches the flow situation. The wall is a perfect heat conductor fixed at temperature $T = T_w$. This induces a thermocapillary Marangoni effect which affects the free surface and fluid flow.

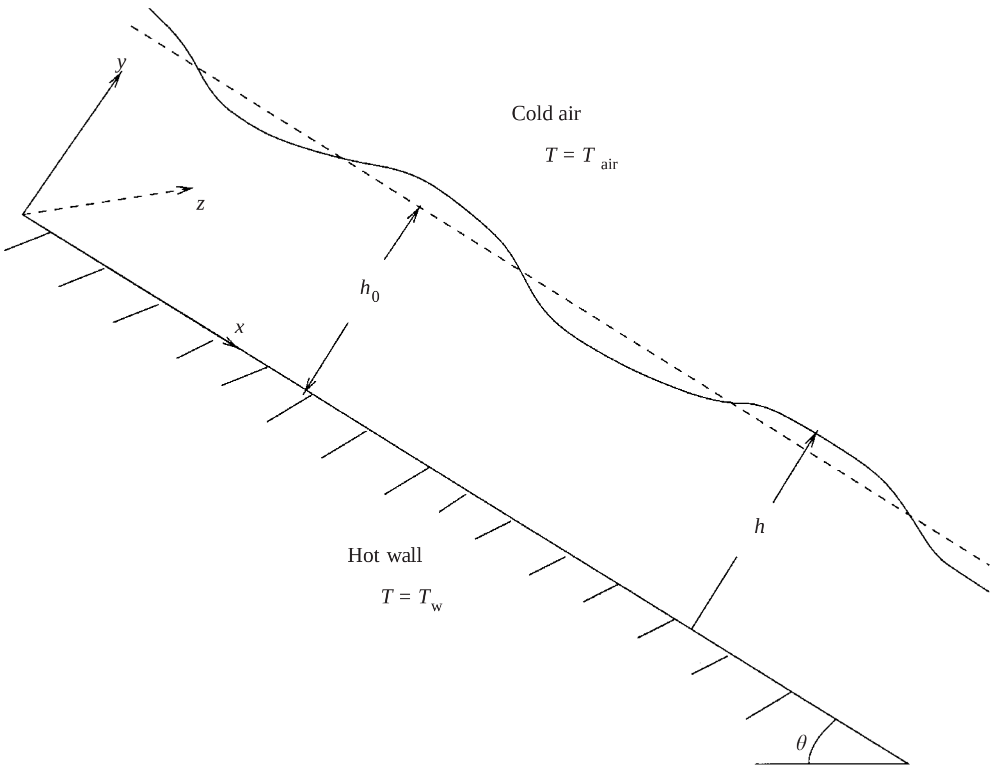

FIGURE 1. Sketch of the profile geometry for flow down a heated inclined plane. The local film thickness is $h(x, z, t)$; h_0 is the average film thickness.

Because of the extreme complexity of the full Navier–Stokes equation with nonlinear free-surface boundary conditions, most nonlinear studies on thin film flows (with and without Marangoni effects) have been based on the long-wave lubrication approximation first developed by Benney (1966) (see also the review by Oron, Davis & Bankoff 1997). As was shown by Salamon, Armstrong & Brown (1993) and Ramaswamy, Chippada & Joo (1996) who compared the long-wave expansion with the full Navier–Stokes equation, Benney's approximation is exact in the limit $Re \ll 1$ but it breaks down at an $O(1)$ Reynolds number. With this approximation, the Navier–Stokes equation reduces to a single, highly nonlinear, partial differential equation commonly known as the evolution equation for the location of the interface. In this study we adopt the integral-boundary-layer approximation (IBL) first introduced by Shkadov (1967). Unlike the usual long-wave lubrication approximation, where relative orders of the film amplitude and the governing dimensionless groups are assigned *a priori*, the IBL equation is derived with only the long-wave expansion and without overly restrictive limitations on the order of the amplitude and the dimensionless groups. The original IBL approximation, though, was restricted to free-surface thin-film flows in the absence of thermal effects. The approximation was recently extended by Kalliadasis *et al.* (2003) to include heat transport effects and to obtain an averaged energy equation for the temperature distribution on the free surface of a film heated from below by a local heat source, $T_w = f(x)$. We follow a similar approach for the problem of a film falling down a wall maintained at constant temperature. The derivation of the IBL approximation in this case parallels the one given by Kalliadasis *et al.* (2003) and the reader is referred to that study for details.

The starting point of the IBL approach is to assume long waves in both the x- and z-directions, i.e. $\partial/\partial x$, $\partial/\partial z \ll \partial/\partial y$ and $v, w \ll u$ with u, v and w the x, y and z components of velocity respectively. The full system of Navier–Stokes/energy equations and wall/free-surface boundary conditions has the trivial solution $h = h_0$, $u^0 = (g \sin\theta/\nu)[h_0 y - (y^2/2)]$, $v = w = 0$, and $T^0 = T_s^0(y/h_0)$ with the temperature at $y = h_0$ given by $T_s^0 = (\lambda h_0/k)T_{\mathrm{air}}/[1 + (\lambda h_0/k)]$ where g is the gravitational acceleration and $\nu = \mu/\rho$ the kinematic viscosity. Also, k is the thermal conductivity of the liquid phase and λ the heat transfer coefficient describing the rate of heat transport from the liquid to the ambient gas phase at the constant temperature T_{air} through the long-wave approximation of Newton's law of cooling at the interface: $k\partial T/\partial y + \lambda(T - T_{\mathrm{air}}) = 0$. Notice that without loss of generality we assume $T_w = 0$ which of course implies $T_s^0 < 0$ and $T_{\mathrm{air}} < 0$, i.e. cooling from the wall side and setting $T_w = 0$ thus makes the surface and air temperatures positive, and excludes the possibility of thermocapillary destabilization of the interface.

We can now utilize the trivial solution to introduce the non-dimensionalization

$$(x, y, z) \to (x, y, z)h_0, \quad h \to hh_0, \quad (u, v, w) \to (u, v, w)u_0,$$
$$t \to \frac{h_0}{u_0}t, \quad P \to \rho u_0^2 P, \quad T \to T\left(-T_s^0\right),$$

where $u_0 = gh_0^2 \sin\theta/3\nu$ is the average velocity of the flat film, h_0/u_0 the time an interfacial particle tranverses a distance h_0 and P the pressure. Note that we can either use a long scale in the x- and z-directions and h_0 in the y-direction to non-dimensionalize the momentum/energy equations and derive the leading-order long-wave equations or simply neglect from the outset the higher-order terms and write down only the leading-order terms of the dimensional momentum/energy equations followed by non-dimensionalization of all lengthscales with h_0. After all, we do know that, to leading order, viscous diffusion in the y-direction must balance inertia and the pressure gradient. Both approaches lead to the same dimensionless equations. Of course, it would seem that scaling all lengths with h_0 (this is effectively the scaling used originally by Shkadov) would imply that the slope of our waves is $O(1)$. However, we shall demonstrate in § 5 that in all cases our solitary waves do obey the long-wave assumption.

In terms of the above non-dimensional variables, the equations of motion, energy equation and wall/free-surface boundary conditions are identical to those given by Kalliadasis *et al.* (2003) with $f \equiv 0$. The governing dimensionless groups, namely the Reynolds, Weber, Péclet, Marangoni and Biot numbers, in terms of the parameters of the problem considered here, are given by

$$Re = \frac{1}{3}\frac{gh_0^3}{\nu^2}\sin\theta, \tag{1a}$$

$$We = \frac{\sigma_0}{\rho h_0 u_0^2} = \frac{3^2\sigma_0\nu^2}{\rho g^2 h_0^5(\sin\theta)^2} = \frac{3^{1/3}\gamma}{Re^{5/3}(\sin\theta)^{1/3}}, \tag{1b}$$

$$Pe = Re\,Pr = Re\frac{\nu}{a}, \tag{1c}$$

$$Ma = \frac{\kappa\left(-T_s^0\right)}{\mu u_0} = \frac{3\kappa\left(-T_s^0\right)}{\rho g h_0^2 \sin\theta}, \tag{1d}$$

$$Bi = \frac{\lambda h_0}{k}, \tag{1e}$$

where σ_0 denotes the surface tension at a reference temperature T_0, $a = k/\rho c_P$ the thermal diffusivity with c_P the constant-pressure heat capacity, and κ is defined from the linear approximation for the surface tension $\sigma = \sigma_0 - \kappa(T_s - T_0)$ ($\kappa > 0$ for typical liquids). The Weber number here expresses the relative importance of surface tension and inertia forces; $\gamma = \sigma_0 \rho^{-1} \nu^{-4/3} g^{-1/3}$ is the Kapitza number, a popular parameter among the Russian school, which is a function of the fluid properties only and not the flow conditions. Pr is the Prandtl number and Pe the Péclet number that expresses the relative importance of convection and conduction. Finally, the Marangoni number expresses the relative importance of thermocapillary and viscous stresses.

Our system is therefore governed by five dimensionless groups: Re, We, Ma, Bi and Pr. Since there is a large number of parameters, a complete investigation over the entire parameter space is almost an impossible task. However, we can reduce the number of relevant dimensionless groups by fixing the liquid and expressing our groups in terms of parameters which depend only on the physical properties of the liquid. For example,

$$Re = \frac{2}{3}\chi \sin\theta, \quad Ma = \frac{3}{2\chi^{2/3}\sin\theta}\frac{B\chi^{1/3}}{1 + B\chi^{1/3}}M,$$

$$Bi = B\chi^{1/3}, \quad We = \frac{9\gamma}{2^{5/3}}\frac{1}{\chi^{5/3}(\sin\theta)^2},$$

where

$$\chi = \frac{g h_0^3}{2\nu^2}, \quad M = \frac{\kappa(-T_{\mathrm{air}})}{\rho}\left(\frac{2}{g\nu^4}\right)^{1/3}, \quad B = \frac{\lambda}{k}\left(\frac{2\nu^2}{g}\right)^{1/3}$$

are the Reynolds, Marangoni and Biot numbers respectively adopted by Goussis & Kelly. Notice that M and B are independent of h_0 and depend only on the physical properties of the liquid phase (like the Kapitza number γ), the heat transfer coefficient of the liquid–gas interface and the temperature difference $T_w - T_{\mathrm{air}}$ (recall that we set $T_w = 0$ such that $T_{\mathrm{air}} < 0$). Hence, for a given liquid–gas system the only relevant parameters are χ, M and inclination angle θ (and the vertical-plane case is a two-parameter problem only).

If the liquid phase is water at 25 °C, $\kappa = 5 \times 10^{-5}\,\mathrm{kg\,s^{-2}\,K^{-1}}$, $k = 0.607\,\mathrm{W\,m^{-1}\,K^{-1}}$, $c_P = 4.18\,\mathrm{J\,g^{-1}\,K^{-1}}$, $\mu = 10^{-2}\,\mathrm{g\,cm^{-1}\,s^{-1}}$, $\rho = 1\,\mathrm{g\,cm^{-3}}$ and $\sigma = 61\,\mathrm{dyn\,cm^{-1}}$ (see for example Reid, Prausnitz & Sherwood 1977). This gives $Pr \simeq 7$ and $\gamma \simeq 3000$. Regarding the Biot number, in the absence of experimental data for heat transfer coefficients at liquid–gas interfaces, we assume the value $B = 10$ taken by Goussis & Kelly. Note that our definition $Bi = \lambda h_0/k$ implies that Bi is proportional to the film thickness h_0 with the proportionality coefficient λ/k a function of the fluid properties. This dependence on h_0 has been made explicit by Goussis & Kelly who, as we pointed out above, used B as the Biot number. Hence, changing h_0 or equivalently the Reynolds number implies changing Bi (although we are not aware of any experimental data which confirm the relationship $Bi \sim \chi^{1/3}$). Finally, for water at 25 °C, $M \simeq 2.45\Delta T$ where ΔT is in K. Hence, for a temperature difference $\Delta T = 10\,\mathrm{K}$, well within an achievable range, we obtain $M \simeq 25$.

The governing equations and boundary conditions can then be simplified using the self-similar profile introduced by Kalliadasis *et al.* (2003). The basic assumption here is that a parabolic velocity profile which satisfies the x-component of the equation of motion for zero Reynolds number persists even for moderate Reynolds numbers when the free surface is no longer flat. Therefore, the variation in the direction of flow is assumed to be slow compared to that in the normal and transverse directions (the same is also true for the long-wave theory). As a consequence, the viscous dissipation depends on a single space variable. This assumption is obviously violated at larger Reynolds numbers where the second-order viscous terms in the normal and transverse directions neglected here become important.

The assumption of a parabolic velocity profile for small to moderate Reynolds numbers is in agreement with the numerical studies by Geshev & Ezdin (1985) and Demekhin, Kaplan & Shkadov (1987) who solved numerically the boundary-layer equations (which unlike IBL do not require any *a priori* assumptions for the velocity profile) and found that for $Re \sim 10$–30 the parabolic profile is a good approximation throughout a solitary wave except in a small neighbourhood of a 'dimple' that develops in front of the solitary hump where a deviation from the parabolic profile was observed. (This dimple is the first in a series of bow waves that connect the steep front edge of a solitary wave to the flat film ahead.) We note that it is well known that wave evolution in a falling film for moderate Reynolds numbers is characterized by a train of soliton-like coherent structures with almost the same amplitude and which interact indefinitely with each other (see Chang 1994 for a review). The parabolicity of the velocity profile has also been verified experimentally for falling liquid films (Alekseenko, Nakoryakov & Pokusaev 1994) in the regime of moderate Reynolds numbers. Measurements of the velocity profile in these solitary waves indicate that the profile is parabolic throughout except perhaps in a small neighbourhood of the dimple.

This velocity profile is substituted into the momentum equations which are then integrated from $y=0$ to $y=h$. The final result is (see Kalliadasis *et al.* 2003 for details)

$$\frac{\partial q}{\partial t}+\frac{6}{5}\frac{\partial}{\partial x}\frac{q^2}{h}+\frac{6}{5}\frac{\partial}{\partial z}\frac{qp}{h}+\frac{3\cot\theta}{Re}h\frac{\partial h}{\partial x}=Weh\frac{\partial K}{\partial x}+\frac{3}{Re}\left(h-\frac{q}{h^2}\right)-\frac{3Ma}{2Re}\frac{\partial T_s}{\partial x}, \tag{2a}$$

$$\frac{\partial p}{\partial t}+\frac{6}{5}\frac{\partial}{\partial x}\frac{qp}{h}+\frac{6}{5}\frac{\partial}{\partial z}\frac{p^2}{h}+\frac{3\cot\theta}{Re}h\frac{\partial h}{\partial z}=Weh\frac{\partial K}{\partial z}-\frac{3}{Re}\frac{p}{h^2}-\frac{3Ma}{2Re}\frac{\partial T_s}{\partial z}, \tag{2b}$$

$$\frac{\partial h}{\partial t}+\frac{\partial q}{\partial x}+\frac{\partial p}{\partial z}=0, \tag{2c}$$

where q and p are the flow rates in the x- and z-directions respectively, T_s the temperature of the interface and K the curvature of the free surface in the long-wave approximation, i.e. $K=h_{xx}+h_{zz}$.

Let us now turn to the IBL treatment of the energy equation. This was discussed by Kalliadasis *et al.* (2003) and the averaged energy equation here is identical to the one obtained in that study by setting $f=0$. Here we show that the IBL treatment of the energy equation adopted by Kalliadasis *et al.* (2003) is effectively a 'tau' method. Like the momentum equations, the first step is the assumption of a self-similar temperature profile

$$T(x,y,z,t)=b(x,z,t)g(\eta),$$

where the amplitude b and the test function g have to be specified. Such a functional form was originally proposed by Zeytounian (1998) for the case $Bi=0$. Zeytounian used for the amplitude b the averaged temperature across the film $\int_0^h T\,\mathrm{d}y$. Here we choose to put the emphasis on the temperature at the interface T_s since it appears directly in Newton's law of cooling and the assumed velocity profile. Therefore, $b\equiv T_s$ and $g(1)=1$. In fact, like the velocity profiles, we choose the temperature profile corresponding to the flat-film solution:

$$T = T_s \eta. \tag{3}$$

Hence, the assumption here is that the linear temperature profile obtained for a flat film $T^0 = T_s^0(y/h_0)$ persists even when the interface is no longer flat. It is clear that this temperature distribution does not satisfy Newton's law of cooling, in fact this mixed Dirichlet–Neumann boundary condition cannot be satisfied simply by choosing g. Hence, in weighted residual methods terminology, the approximation in (3) is a variant of the Galerkin method invented by Lanczos, called the 'tau' method (Gottlieb & Orszag 1977), in which the trial function does not satisfy the equation or (all) boundary conditions. Integrating the energy equation from $y=0$ to $y=h$ shows that the usual Kármán–Pohlhausen method cannot be applied for the energy equation as it was for the momentum equation. Let us take for example the dissipative term whose integration over the film thickness yields

$$\int_0^h T_{yy}\,\mathrm{d}y = T_y|_{y=h} - T_y|_{y=0}.$$

The gradient on the interface $T_y|_{y=h}$ is given by Newton's law of cooling; however the gradient on the wall is unknown. This difficulty can be easily overcome by simply applying a weight function $W(\eta)$ with $\eta = y/h$ to the energy equation before its averaging. After integrating by parts, the diffusive term now becomes

$$\int_0^h W\left(\frac{y}{h}\right) T_{yy}\,\mathrm{d}y = \left[W\left(\frac{y}{h}\right) T_y\right]_0^h - \frac{1}{h}\left[W'\left(\frac{y}{h}\right) T\right]_0^h + \frac{1}{h^2}\int_0^h W''\left(\frac{y}{h}\right) T\,\mathrm{d}y.$$

Notice that taking W to be the parabolic profile $2\eta - \eta^2$ gives

$$\int_0^h (2\eta - \eta^2) T_{yy}\,\mathrm{d}y = T_y|_{y=h} - \frac{2}{h^2}\int_0^h T\,\mathrm{d}y$$

which leads to the choise made by Zeytounian (1998) of an amplitude corresponding to the averaged temperature across the flow. In our case, the weight function is taken to be linear, $W = \eta$. The averaged diffusive term then becomes

$$\int_0^h \eta T_{yy}\,\mathrm{d}y = T_y|_{y=h} - \frac{1}{h}(T_s - T|_{y=0}) \equiv -Bi(T_s - T_{\mathrm{air}}) - \frac{1}{h} T_s.$$

Hence, we multiply the energy equation with the weight function η, we perform integrations by parts and evaluate the boundary terms which involve T_y from Newton's law of cooling and not (3) (which of course does not satisfy Newton's law of cooling). Thus we apply all boundary conditions prior to substituting the linear approximation in (3). As a result, although (3) does not satisfy the free-surface boundary condition, the averaged energy equation does. The final averaged energy equation is

$$\frac{\partial T_s}{\partial t} + \frac{7}{40}\frac{T_s}{h}\left(\frac{\partial q}{\partial x} + \frac{\partial p}{\partial z}\right) + \frac{27}{20}\frac{q}{h}\frac{\partial T_s}{\partial x} + \frac{27}{20}\frac{p}{h}\frac{\partial T_s}{\partial z} + \frac{3}{Pe}\left[\frac{Bi(T_s - T_{\mathrm{air}})}{h} + \frac{T_s}{h^2}\right] = 0. \tag{4}$$

Equations ($2a$–c) and (4) are the basic equations for the analysis to follow.

3. Linear stability of the trivial solution

The system of equations (2*a*–*c*), (4) admits the trivial solution

$$h = 1, \quad q = 1, \quad p = 0, \tag{5a}$$

$$T_s = -1, \quad T_{\text{air}} = -\frac{1 + Bi}{Bi}. \tag{5b}$$

We consider the stability of this solution to three-dimensional infinitesimal perturbations in the form of normal modes:

$$h = 1 + \hat{h} \exp[\mathrm{i}(\alpha x + \beta z - \omega t)], \tag{6a}$$

$$q = 1 + \hat{q} \exp[\mathrm{i}(\alpha x + \beta z - \omega t)], \tag{6b}$$

$$p = \hat{p} \exp[\mathrm{i}(\alpha x + \beta z - \omega t)], \tag{6c}$$

$$T_s = -1 + \hat{T} \exp[\mathrm{i}(\alpha x + \beta z - \omega t)]. \tag{6d}$$

Substituting (6) into (2*a*–*c*), (4) and linearizing for $\hat{h}$, $\hat{q}$, $\hat{p}$, $\hat{T} \ll 1$, yields the disturbance equations

$$-\mathrm{i}\omega\hat{q} + \frac{6}{5}\mathrm{i}\alpha(2\hat{q} - \hat{h}) + \frac{6}{5}\mathrm{i}\beta\hat{p} + \frac{3\cot\theta}{Re}\mathrm{i}\alpha\hat{h} = -\mathrm{i}\alpha(\alpha^2 + \beta^2)We\hat{h} + \frac{3}{Re}(3\hat{h} - \hat{q}) - \frac{3Ma}{2Re}\mathrm{i}\alpha\hat{T}, \tag{7a}$$

$$-\mathrm{i}\omega\hat{p} + \frac{6}{5}\mathrm{i}\alpha\hat{p} + \frac{3\cot\theta}{Re}\mathrm{i}\beta\hat{h} = -\mathrm{i}\beta(\alpha^2 + \beta^2)We\hat{h} - \frac{3}{Re}\hat{p} - \frac{3Ma}{2Re}\mathrm{i}\beta\hat{T}, \tag{7b}$$

$$-\mathrm{i}\omega\hat{h} + \mathrm{i}\alpha\hat{q} + \mathrm{i}\beta\hat{p} = 0, \tag{7c}$$

$$-\mathrm{i}\omega\hat{T} - \frac{7}{40}\mathrm{i}(\alpha\hat{q} + \beta\hat{p}) + \frac{27}{20}\mathrm{i}\alpha\hat{T} + \frac{3}{Pe}[(1 + Bi)\hat{T} + \hat{h}] = 0, \tag{7d}$$

which form a linear algebraic system with constant coefficients. For the system to have non-trivial solutions it is necessary and sufficient that its principal determinant be equal to zero. This yields an algebraic eigenvalue problem of the form

$$\det||\boldsymbol{A} - \mathrm{i}\omega\boldsymbol{I}|| = 0$$

for the eigenvalue ω, where $\boldsymbol{A}$ is a 4×4 matrix and $\boldsymbol{I}$ is the unitary matrix. This is the dispersion relationship for ω as a function of α and β. Notice that the three-dimensional stability problem defined by system (7) cannot be transformed to an equivalent two-dimensional problem and hence Squire's theorem is not valid for thin films in the presence of thermocapillary Marangoni effects.

The case of a thin liquid film falling down an inclined plane in the absence of Marangoni effects deserves special attention: clearly from (2*a*–*c*), (4) with $M = 0$, the hydrodynamic and thermal problems are decoupled, so that the temperature field does not have any effect on the film thickness. The energy equation by itself is of the diffusion-type and hence cannot induce instability. Therefore, *Bi*, although important for the temperature field, does not affect the stability boundary for $M = 0$. With (7*d*) decoupled from (7*a*–*c*), the dispersion relation can be readily obtained analytically: multiply (7*a*) by α and (7*b*) by β and add the resulting equations. The new equation contains the term $\alpha\hat{q} + \beta\hat{p} = \omega\hat{h}$ from (7*c*) (notice that for $M \neq 0$ the linearized energy equation in (7*d*) has some terms not proportional to $\alpha\hat{q} + \beta\hat{p}$ and that is why Squire's transformation does not work in this case). Separating real and imaginary parts and

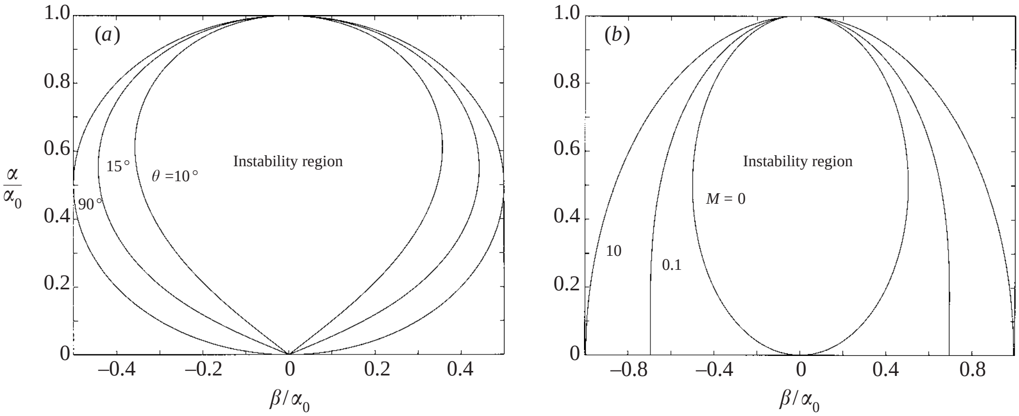

FIGURE 2. Neutral curve for stability of a flat film with respect to three-dimensional distrurbances. α_0 is the neutral wavenumber for two-dimensional disturbances. In all our calculations for figures 2–4, $\gamma = 3000$, $Pr = 7$, $B = 10$. (*a*) $\chi = 10$, $M = 0$ and three different inclination angles, 90°, 15° and 10°; (*b*) $\chi = 0.1$, $\theta = 90°$ and three different Marangoni numbers, $M = 0$, 0.1 and 10.

setting $\omega_I = 0$ yields the neutral curve

$$(\alpha^2 + \beta^2)^2 We = 3\alpha^2 - \frac{3\cot\theta}{Re}(\alpha^2 + \beta^2) \tag{8a}$$

with a phase velocity

$$c_0 = 3 \tag{8b}$$

and such that the neutral wavenumber for two-dimensional waves is

$$\alpha_0 = \sqrt{\frac{3}{We}\left(1 - \frac{\cot\theta}{Re}\right)}. \tag{8c}$$

Notice that as a consequence of Squire's transformation for $M = 0$, the most unstable disturbance is a two-dimensional one; obviously, in the nonlinear regime this might no longer be the case.

For a vertical film, (8*a*) gives the expected result for the neutral curve

$$(\alpha^2 + \beta^2)^2 We = 3\alpha^2$$

first obtained by Demekhin & Shkadov (1984). This curve has two branches in the (α, β)-plane: $\alpha^2 + \beta^2 = \pm(3/We)^{1/2}\alpha$. The two branches are the miror image of each other with respect to the β-axis but the one with the negative sign does not have physical meaning. The branch with the positive sign is shown in figure 2(*a*) where both α and β are normalized with the neutral wavenumber for two-dimensional waves given by (8*c*). For $\theta = \pi/2$ both branches are circles while for $\theta < \pi/2$ the neutral curve takes on a 'figure-of-eight' shape. The effect of inclination angle on the neutral curve is shown in the figure: by reducing θ the instability region shrinks and three-dimensional effects become weaker, as was first shown by Demekhin & Shkadov (1984). As θ decreases the stability boundary is stretched in the α-direction and eventually, for $\theta = 0$, degenerates to a straight line parallel to that direction.

For $M \neq 0$, the eigenvalue problem in (7) has to be solved numerically. Figure 2(*b*) depicts the stability boundary for three-dimensional disturbances on a vertical falling film in the presence of Marangoni effects. The instability region in the β-direction increases as M increases and hence the Marangoni effects enhance the three-dimensional instability. Now, since Squire's transformation is no longer valid, there is a possibility that three-dimensional waves might be more unstable than two-dimensional. But for this purpose, M has to be large enough, since for $M \ll 1$ we anticipate that the system will behave in a fashion similar to the $M = 0$ case. A complete investigation of this issue is beyond the scope of the present study. Note, however, that Goussis & Kelly (1991) showed that two regions of Marangoni instability (interfacial waves and cells) coalesce into one region for certain values of the governing parameters and it is reasonable to expect that exactly at this point three-dimensional waves might be more unstable.

For the remainder of our study we shall consider only two-dimensional disturbances ($\beta = 0$). In this case we can obtain an explicit form for the dispersion relation:

$$\alpha^2 c^3 + d_2 c^2 + d_1 c + d_0 = 0, \tag{9}$$

where

$$d_2 = \frac{1}{4Pe\,Re}[12\mathrm{i}\alpha Pe - 15\alpha^2 Re\,Pe + 12\mathrm{i}\alpha Re(1 + Bi)],$$

$$d_1 = \frac{1}{400Pe\,Re}[105Ma\alpha^2 Pe - 1200\alpha^2 Pe\cot\theta - 400\alpha^4 We\,Re\,Pe - 5220\mathrm{i}\alpha Pe - 3600(1 + Bi) - 2880\mathrm{i}\alpha Re(1 + Bi) - 1776\alpha^2 Re\,Pe],$$

$$d_0 = \frac{1}{400Pe\,Re}[1440\mathrm{i}\alpha Re(1 + Bi) + 1800\mathrm{i}\alpha Ma + 4860\mathrm{i}\alpha Pe + 10800(1 + Bi) + 1620\alpha^2 Pe\cot\theta - 3600\mathrm{i}\alpha\cot\theta(1 + Bi) - 648\alpha^2 Re\,Pe + 540\alpha^4 We\,Re\,Pe - 1200\mathrm{i}\alpha^3 We\,Re(1 + Bi)].$$

Let us now obtain the critical condition for the onset of instability when $\beta = 0$. For this purpose we expand the phase velocity as

$$c \sim c_0 + \mathrm{i}\alpha c_1 + \alpha^2 c_2 + \mathrm{i}\alpha^3 c_3 \tag{10a}$$

(it turns out that even terms of this expansion are real and odd purely imaginary) which when substituted in (9) yields

$$c_1 = Re + \frac{Ma}{2(1 + Bi)} - \cot\theta, \tag{10b}$$

$$c_2 = \frac{6}{5}Re\left(\cot\theta - Re - \frac{Ma}{2(1 + Bi)}\right) + \frac{Ma\,Pe}{16(1 + Bi)^2}\left(\frac{7}{5}Bi - 3\right), \tag{10c}$$

$$c_3 = -\frac{133}{75}Re^3 + \frac{7}{480}\frac{Ma^2 Pe}{(1 + Bi)^2} - \frac{1}{12}\frac{Ma^2 Pe}{(1 + Bi)^3} + \frac{77}{1600}\frac{Ma\,Pe^2}{1 + Bi} - \frac{121}{800}\frac{Ma\,Pe^2}{(1 + Bi)^3} - \frac{1}{3}We\,Re - \frac{1}{3}Re(\cot\theta)^2 + \frac{1}{3}\frac{Ma\,Re\cot\theta}{1 + Bi} - \frac{1}{12}\frac{Ma^2 Re}{(1 + Bi)^2} + \frac{158}{75}Re^2\cot\theta - \frac{79}{75}\frac{Ma\,Re^2}{1 + Bi} - \frac{149}{300}\frac{Ma\,Re\,Pe}{(1 + Bi)^2} + \frac{161}{1200}\frac{Ma\,Re\,Pe}{1 + Bi} + \frac{1}{6}\frac{Ma\,Pe\cot\theta}{(1 + Bi)^2} - \frac{7}{240}\frac{Ma\,Pe\cot\theta}{1 + Bi}, \tag{10d}$$

with $c_0 = 3$ as expected from (8). Equation (9) has three roots for the eigenvalue c. The expansion in (10) gives the only root that can become unstable. The other two roots are always stable and will be discussed later on. From $\omega_I = \alpha c_I \sim \alpha^2 c_1 + \alpha^4 c_3 + \cdots$, the onset of instability occurs at $c_1 = 0$ which gives the critical condition

$$Re + \frac{Ma}{2(1+Bi)} = \cot\theta. \tag{11a}$$

This relation defines the critical Reynolds number, $Re^* = \cot\theta - Ma/(2(1+Bi))$, above which the flow loses stability. For $Ma = 0$, $Re^* = \cot\theta$ (alternatively, set the neutral wavenumber in (8*c*) equal to zero). In terms of the variables χ, M and B introduced in the previous Section, (11*a*) can be written as

$$(\chi \sin\theta)^2 + \frac{9}{8}\frac{M\chi^{1/3}}{(1+B\chi^{1/3})} = \frac{3}{2}\chi\cos\theta. \tag{11b}$$

This condition has the same functional form as the one derived by Goussis & Kelly (1991) for two-dimensional waves at criticality, but the coefficients are slightly different: 9/8 and 3/2 instead of 15/16 and 5/4 obtained by Goussis & Kelly, i.e. a 20% error. A similar discrepancy is found for the critical Reynolds number predicted by IBL in the absence of Marangoni effects, i.e. $\cot\theta$, instead of $(5/6)\cot\theta$ as obtained by a direct Orr–Sommerfeld stability analysis of the full Navier–Stokes equations and by the usual long-wave lubrication approximation. In fact, IBL does not predict very accurately neutral and critical conditions, except for large inclination angles; indeed for a vertical falling film, and in the absence of Marangoni effects, $Re^* = 0$ so that the flow is unstable for all Reynolds numbers. For all other inclination angles, IBL introduces an error that increases as the inclination angle decreases (however, IBL does capture qualitatively the linear stability properties of the system). The discrepancy is simply due to the velocity profile assumed in the Galerkin expansion of the Skhadov method: self-similar parabolic profile across the film (see also the discussion by Ruyer-Quil & Manneville 2002). Although this profile seems to be in agreement with the experiments by Alekseenko *et al.* (1994), and hence does capture most of the physics, corrections to the profile, known already to exist at first order in the film parameter from the long-wave expansion, are important for an accurate prediction of the linear instability threshold. Such corrections in the absence of Marangoni effects have been obtained by Ruyer-Quil & Manneville (1998, 2000, 2002) for the falling film problem using high-order Galerkin expansions. These higher-order IBL models accurately predict conditions at criticality. Ruyer-Quil *et al.* (2003) have recently developed such higher-order models for the falling film problem in the presence of Marangoni effects.

Far from criticality the neutral curve must be obtained numerically. Figure 3(*a*) depicts the neutral stability curve for a vertical falling film with $\gamma = 3000$, $Pr = 7$, $B = 10$ and different temperature differences ΔT, or Marangoni numbers M. The instability region is located above the neutral curve. In addition to the curves shown in the figure, $\alpha = 0$ is also a neutral curve. For $M = 0$ and as $\chi \to 0$ ($Re \to 0$) the neutral wavenumber also approaches zero. With $M > 0$, the region of instability increases. Now as $\chi \to 0$, the neutral wavenumber α_0 does not tend to zero but the neutral curves intersect the α-axis at values that increase as M increases. Indeed, for a vertical falling film and in the absence of Marangoni effects, the destabilizing inertia terms are vanishing as $Re \to 0$, but for $M \neq 0$ and as $Re \to 0$ the destabilizing forces are surface forces which are still present for small Re. As is also evident from the figure, the influence of the Marangoni instability is larger for small χ or small thicknesses where the neutral wavenumber is finite.

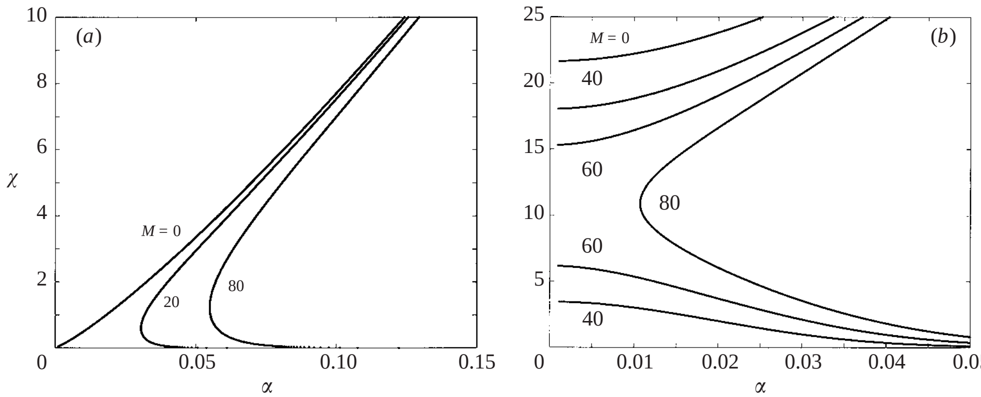

FIGURE 3. Neutral stability curves for different Marangoni numbers, M. (a) $\theta = 90°$. The instability region is located above the neutral curves; (b) $\theta = 15°$. For $M = 40$, 60 the instability region is located above the upper neutral curve and below the lower neutral curve. For $M = 80$, the instability region is located to the left of the neutral curve. The stability curves for $M = 40$ and $M = 60$ can be continued in the $\alpha \to 0$ regime by using the critical condition in (11b).

Let us note that the long-wave expansion for the dispersion relation in (10a) predicts that the neutral wavenumber α_0 with zero growth rate occurs at zero wavenumber and at $\sqrt{-(1/c_3)(Re - Re^*)}$ (for small wavenumbers and hence small $Re - Re^*$) so that $\alpha_0 \to 0$ as $Re - Re^* \to 0$. Hence, the instability is a long-wave variety with a maximum growing linear mode at criticality with a wavenumber that is exactly zero. However, from figure 3(a), for $\theta = \pi/2$ and $M \neq 0$, α_0 is finite and does not tend to zero near criticality, i.e. as $\chi \to 0$. Hence, (10a) is valid only for $M = 0$ when $\theta = \pi/2$.

Figure 3(b) shows the neutral stability curves for an inclined plane with $\theta = 15°$. Again, $\alpha = 0$ is also a neutral curve. For $M = 0$ there is only one region of instability, located above the neutral curve. This is the well-known surface instability that occurs if the Reynolds number is larger than a critical value ($\equiv \cot\theta$ from (11a)). For finite M there exists a second region of instability if χ is smaller than a certain value. Instability now occurs above the upper neutral curve and below the lower neutral curve. The χ values at which the two branches of the neutral curve intersect the χ-axis for finite M can be easily obtained from (11b). As M increases these two values approach each other and eventually at a sufficiently large M the two χ values are the same. For larger values of M the two branches merge into one and now the film is unstable for all values of χ, at least for large-wavelength disturbances (the instability region is located to the left of the neutral curve). These results were first obtained by Goussis & Kelly (1991). Comparison with the neutral stability curves in the Goussis & Kelly study show that IBL captures well the variation of the stability boundaries with α and M. There is, however, a difference between our neutral curves in figure 3(b) and the original curves in the Goussis & Kelly study with a maximum error introduced by IBL of the order of 20%.

The long-wave expansion for the dispersion relation in (10a) is valid near the critical points of the stability boundaries in figure 3(b) (these are the points where the neutral stability curves intersect the χ-axis) or when the single neutral stability curve in figure 3(b) (for M larger than a critical value) is very close to the χ-axis. But as was remarked above, (10a) is not valid as $\chi \to 0$ since the neutral wavenumber does not tend to zero. However, the lower critical point (the point where the lower

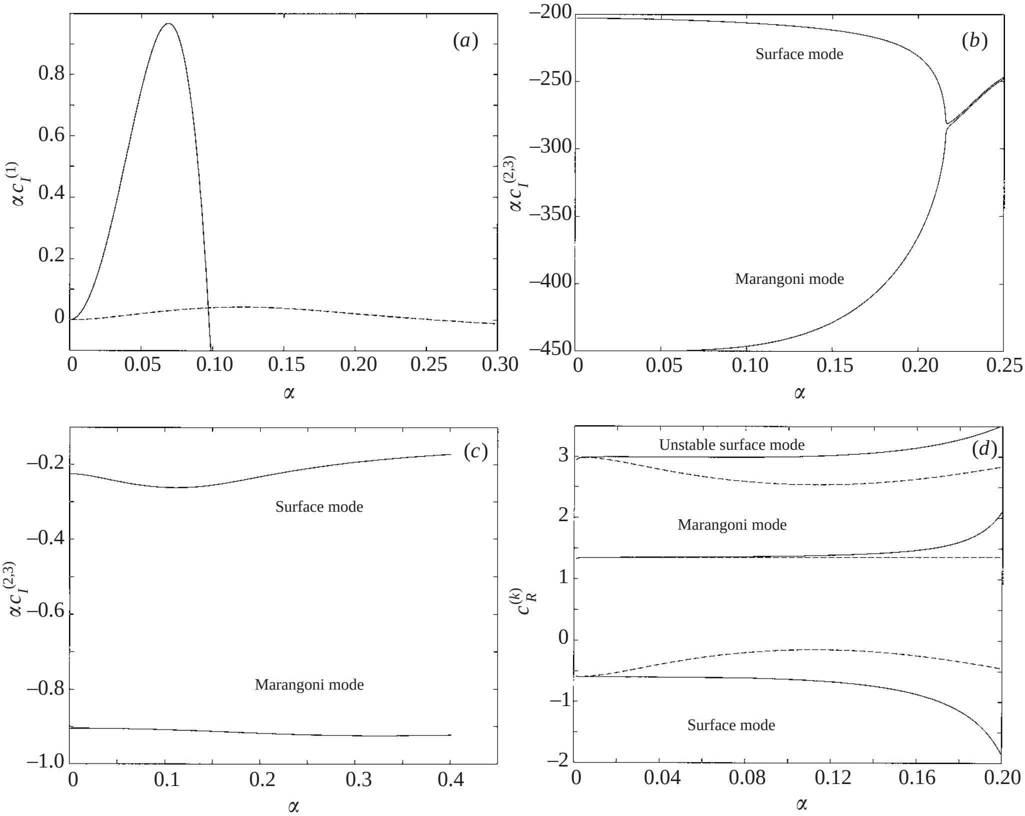

FIGURE 4. (a) Growth rate, $\alpha c_I^{(1)}$, of the surface mode propagating downstream with $\theta = 90°$ and $M = 80$. The solid line is for $\chi = 0.01$ and the dashed line for $\chi = 20$. The maximum growth rate for $\chi = 20$ is 0.04 – contrast with a maximum growth rate of $\simeq 1$ for $\chi = 0.01$. (b) Growth rates, $\alpha c_I^{(2,3)}$, for the upstream propagating surface mode and Marangoni mode with $\theta = 90°$, $\chi = 0.01$ and $M = 80$. (c) Growth rates for the upstream propagating surface mode and Marangoni mode with $\theta = 90°$, $\chi = 20$ and $M = 80$. (d) Phase velocity, $c_R^{(k)}$, of all modes for $\theta = 90°$, $\chi = 0.01$ (solid lines), $\chi = 20$ (dashed lines) and $M = 80$.

neutral stability curve intersects the χ-axis) moves towards the origin when $M \to 0$ and $\theta = \pi/2$, so that the expansion in (10a) is also valid for $M = 0$, $\theta = \pi/2$ and $\chi \to 0$.

We now return to the full dispersion relation in (9). Two of the roots correspond to two surface waves propagating downstream and upstream respectively, and the third root is a Marangoni mode. For $M = 0$, this root is obtained from the energy equation which is decoupled from the hydrodynamic problem in this limit. The three roots can then be easily traced as we increase M. Figure 4(a) shows the growth rate αc_I as a function of wavenumber α for the mode propagating downstream with $\theta = 90°$, $M = 80$ and two values of χ. Evidently, for $\chi = 0.01$, this mode is strongly unstable with a maximum growth rate of approximately 1. Hence, the usual interfacial mode in the absence of Marangoni effects is strongly amplified in the region of small χ when Marangoni effects are present, consistent with the neutral stability curves in figure 3(a). This strong instability that manifests itself through large growth rate also implies an interesting behaviour for the nonlinear solutions in the region $\chi \ll 1$. Indeed, we shall demonstrate that both amplitude and speed of the solitary waves in this region blow up at infinity. Notice that the cut-off wavenumber (above which the growth rate is stable) is small and hence the long-wave assumption is not violated. This cut-off wavenumber approaches a limiting value as $\chi \to 0$ with $\alpha = 0$ always a neutral mode, in agreement with figure 3(a).

For the relatively large value $\chi = 20$ where the influence of the Marangoni effect is small, the maximum growth rate now is approximately 0.04, almost 20 times smaller than the maximum growth rate for $\chi = 0.01$. However, the region of unstable wavenumbers is now larger than the one for $\chi = 0.01$. Also, the cut-off wavenumber is small and the long-wave assumption is not violated.

The two other modes are strongly decaying as shown in figures 4(b) and 4(c), with the Marangoni mode decaying faster than the upstream propagating surface mode. In fact, the Marangoni mode is stable for all values of θ, χ and M. Hence, the role of the Marangoni effect is to amplify the usual hydrodynamic mode of instability for $M = 0$ and not to introduce a new unstable mode. Notice that for $\chi = 0.01$ the two roots coalesce at a particular value of α. Finally, the growth rate of the two stable modes tends towards $-\infty$ as criticality is approached. For $\chi = 20$, the growth rates of the two stable modes are now much larger than the ones observed for small χ.

In figure 4(d) we depict the phase velocity, c_R, of all modes for $\theta = 90°$, $M = 80$ and two values of χ. For $\chi = 0.01$, the phase velocity of the unstable mode is close to 3 away from the region of very small wavenumbers, so that these interfacial waves travel steadily downstream with a velocity roughly three times the average velocity of the flat film. However, for very small wavenumbers, the phase velocity deviates from 3 – recall, that the long-wave expansion in (10a) is not valid for $\chi \to 0$ when $\theta = \pi/2$ and $M \neq 0$ and hence the phase velocity of the unstable mode is different from 3 in this region. For $\chi = 0.01$, the second surface mode propagates upstream with $c_R \simeq -0.5$ while the Marangoni mode propagates downstream with $c_R \simeq 1.5$. For $\chi = 20$, the phase velocity of the first mode is close to 3. Notice that for $\chi = 20$, the phase velocity of all three modes is qualitatively similar to that for $\chi = 0.01$.

4. Reduced nonlinear models

4.1. *Kuramoto–Sivashinsky limit*

For the purely hydrodynamic instability with $M = 0$, it is well known that in the vicinity of the point where the neutral stability curve intersects the χ-axis in figure 3(b), a weakly nonlinear long-wave expansion yields the Kuramoto–Sivashinsky (KS) equation first derived by Shkadov (1973) (see also Nepomnyaschy 1974; Lin 1974; and Demekhin, Demekhin & Shkadov (1983)). This expansion is of small amplitude and hence the neutral wavenumber α_0 must be small. However, α_0 can be small with different parameter conditions. One approach, for example, presumes near-critical conditions, $Re \to Re^*$. The derivation of the KS equation for $M = 0$ then typically involves the use of the method of multiple scales, with a small parameter $\epsilon = \alpha_0$ such that $Re - Re^* = O(\epsilon^2)$, and a transformation of the equations in a frame moving with the long-wave linear phase velocity 3.

In our case we have a second critical point where $\alpha_0 = 0$: this is the point where the lower branch of the neutral stability curve in figure 3(b) intersects the χ-axis. The KS equation then applies in the vicinity of the two critical points given by (11) or when the two branches coalesce into a single curve very close to the χ-axis, i.e. $\alpha_0 \to 0$. From the dispersion relation in (10a), $\alpha_0^2 = -(Re - Re^*)/c_3$ and hence there are different possibilities for α_0 to approach zero: (i) $Re - Re^* \to 0$, c_3 fixed; (ii) $c_3 \gg 1$, $Re - Re^*$ fixed; (iii) $Re - Re^* \to 0$ and $c_3 \gg 1$. The magnitude of c_3 is affected by

$We\,Re$, assuming that all other parameters are fixed. Hence, $c_3 \gg 1$ is equivalent to $We\,Re \gg 1$. These different parameter conditions to achieve a small α_0 will in general lead to different weakly nonlinear equations. The derivation of these equations for the falling film problem in the absence of Marangoni effects is discussed in detail by Chang & Demekhin (2002).

A simple derivation of the KS equation can be obtained using an approach suggested by Whitham (1973) for conservative systems of the type considered here, $\partial h/\partial t + \partial q/\partial x = 0$. For such systems one can postulate (on either empirical or theoretical grounds) that there is a functional relation between q and h, $q = q(h)$. This functional relation can be easily obtained from the one-dimensional version of (2a) by setting all time and space derivatives equal to zero, effectively assuming a slow variation in time and space (this assumption can be easily justified for the long-wave instability with $\alpha_0 \to 0$ considered here). We then have

$$q = h^3. \tag{12a}$$

Similarly, from the interface temperature equation (4),

$$T_s = \frac{BiT_{\text{air}}}{1+Bih}h = -\frac{1+Bi}{1+Bih}h. \tag{12b}$$

A better approximation for q and T_s can be obtained by assuming that q, T_s are also functions of the derivatives of h (the assumption that q depends linearly on h and its gradient h_x employed by Whitham leads to Burgers' equation). To obtain these higher-order approximations for q and T_s we consider (2a), (4) in a frame moving with the long-wave linear phase velocity 3 (so that $\partial/\partial t \to \partial/\partial t - 3\partial/\partial x$), since as a first approximation all waves are moving with the speed 3. We further assume that $\partial/\partial t - 3\partial/\partial x \simeq -3\partial/\partial x$ and we set up the iterative schemes

$$q^{n+1} = h^3 + Reh^2\frac{\partial q^n}{\partial x} - \frac{2}{5}Reh^2\frac{\partial}{\partial x}\left(\frac{(q^n)^2}{h}\right) - \cot\theta h^3\frac{\partial h}{\partial x} + \frac{Re\,We}{3}h^3\frac{\partial^3 h}{\partial x^3} - \frac{1}{2}Mah^2\frac{\partial T_s}{\partial x} \tag{13a}$$

and

$$T_s^{n+1} = \frac{BiT_{\text{air}}}{1+Bih}h + Pe\frac{h^2}{1+Bih}\frac{\partial T_s^n}{\partial x} - \frac{7}{120}Pe\frac{h}{1+Bih}T_s^n\frac{\partial q^n}{\partial x} - \frac{9}{20}Peq^n\frac{h}{1+Bih}\frac{\partial T_s^n}{\partial x} \tag{13b}$$

for $n = 0, 1, \ldots$ with q_0 and T_s^0 given by (12). This approximation implies that both q and T_s are adiabatically slaved to h and they depend on time only through the dependence of h on time. For simplicity we take $Ma = O(1)$. At the next approximation with $n = 1$ we obtain

$$q = h^3 + 3Reh^4\frac{\partial h}{\partial x} - 2Reh^6\frac{\partial h}{\partial x} - \cot\theta h^3\frac{\partial h}{\partial x} + \frac{Re\,We}{3}h^3\frac{\partial^3 h}{\partial x^3} - \frac{1}{2}Mah^2\frac{\partial T_s}{\partial x}. \tag{14}$$

For $\alpha_0 \to 0$ the deviation of the interface amplitude from 1 is small. We then substitute $h \sim 1 + \hat{h}$ with $\hat{h} \ll 1$ in (14) to obtain

$$q \sim 1 + 3\hat{h} + 3\hat{h}^2 + Re\hat{h}_x - \cot\theta\hat{h}_x + \frac{We\,Re}{3}\hat{h}_{xxx} - \frac{1}{2}Ma\frac{\partial T_s}{\partial x} \tag{15}$$

so that to leading order $\partial q/\partial t \sim \partial \hat{h}/\partial t \sim -3\partial q/\partial x$, as we assumed in the derivation of (13). Notice that in (15) terms of $O(\hat{h}\hat{h}_x)$ and higher have been neglected. Indeed we can easily show from the long-wave approximation that $\hat{h}\hat{h}_x \ll \hat{h}^2$. Also we have assumed $We\,Re\hat{h}_{xxx} \gg \hat{h}\hat{h}_x$, a condition which will be examined later on once we assign an order of magnitude for all our parameters with respect to α_0. Finally, $T_{sx} \sim \hat{h}_x$ to leading order.

We now substitute $h \sim 1+\hat{h}$ into the first-order correction for the interface temperature from (13*b*) to obtain

$$T_s \sim -1 - \frac{1}{1+Bi}\hat{h} + Peb\hat{h}_x \tag{16a}$$

where

$$b = \frac{7}{40}\frac{1}{1+Bi} - \frac{11}{20}\frac{1}{(1+Bi)^2}. \tag{16b}$$

Substituting (16*a*) into (15) yields

$$q \sim 1 + 3\hat{h} + 3\hat{h}^2 + Re\hat{h}_x - \cot\theta\,\hat{h}_x + \frac{We\,Re}{3}\hat{h}_{xxx} - \frac{1}{2}Ma\,Peb\hat{h}_{xx}. \tag{17}$$

Hence, the $\hat{h}_x$ term in (16*a*) contributes a $\hat{h}_{xx}$ term to the expression for the flow rate. As we have already neglected terms of $O(\hat{h}\hat{h}_x)$ in (14) the term $Ma\,Peb\hat{h}_{xx}$ can be retained at this level of the approximation provided that $Ma\,Peb\hat{h}_{xx} \gg \hat{h}\hat{h}_x$. We shall return to this condition later on when we assign an order of magnitude for the amplitude $\hat{h}$ with respect to α_0. Notice that the only nonlinearity in (17) is $\hat{h}^2$ which originates from the flow rate expression (12*a*).

The kinematic boundary condition in (2*c*), with the moving coordinate transformation $\partial/\partial t \to \partial/\partial t - 3\partial/\partial x$ and $h \sim 1+\hat{h}$, yields

$$\frac{\partial \hat{h}}{\partial t} + 6\hat{h}\frac{\partial \hat{h}}{\partial x} + a_1\frac{\partial^2 \hat{h}}{\partial x^2} + a_2\frac{\partial^4 \hat{h}}{\partial x^4} + a_3\frac{\partial^3 \hat{h}}{\partial x^3} = 0, \tag{18a}$$

where

$$a_1 = Re - \cot\theta + \frac{Ma}{2(1+Bi)} = Re - Re^*, \tag{18b}$$

$$a_2 = \frac{We\,Re}{3}, \tag{18c}$$

$$a_3 = -\tfrac{1}{2}Ma\,Peb = \frac{Ma\,Pe}{16(1+Bi)^2}\left(3 - \tfrac{7}{5}Bi\right). \tag{18d}$$

This equation without the $\hat{h}_{xxx}$ term is the KS equation we seek. With the addition of this term, (18*a*) becomes the generalized KS or Kawahara equation whose solitary wave solutions and time-dependent behaviour have been scrutinized by Kawahara (1983) and Kawahara & Toh (1988). A detailed phase-space analysis of all solitary wave solutions of this equation including multi-hump solitary waves has been performed by Nekorkin & Velarde (1994). The laminarizing effects of dispersion have been analysed in detail by Chang, Demekhin & Kopelevich (1993*a*) who constructed bifurcation diagrams for the periodic and solitary stationary wave solutions of this equation, and also examined their linear stability. Chang, Demekhin & Kopelevich (1995) and Chang, Demekhin & Kalaidin (1998) analysed the response of solitary pulses to radiation wave packet disturbances and showed that pulse–packet interactions are dominated by the spectrum of the pulses. Finally, the Kawahara equation can be viewed as a particular case of the more general Korteweg–de Vries–KS–Velarde equation that describes the evolution of the free surface of Marangoni–Bénard liquid layers heated from above (the equation contains the additional nonlinear term $(\hat{h}\hat{h}_x)_x$). Issues related to existence of solitary wave solutions of this equation and solitary wave interactions/head-on collisions have been addressed by Christov & Velarde (1995) while a detailed review of all these weakly nonlinear prototypes is given by Nepomnyashchy, Velarde & Colinet (2002).

It should be noted that the dispersion relation obtained from (18*a*) yields only one root. This is effectively the usual hydrodynamic mode for a falling film in the absence of Marangoni effects appropriately modified by the Marangoni effects. This mode was discussed in detail in § 3. The other two modes are not captured by our weakly nonlinear expansion which is based on the assumption of a slaved flow rate and temperature field. Equivalently, the two stable roots of the full dispersion relation in (9) are *slave modes* and have been adiabatically eliminated.

Let us now examine the order of magnitude of the various terms in (18*a*). We first consider the possibility $Re - Re^*$ fixed, say $O(1)$, and $c_3 \gg 1$. From (1*b*) this corresponds to $\gamma \gg 1$ (in the derivation of IBL, $We\,Re = O(\epsilon^{-2})$ with respect to the long-wave parameter ϵ that measures the gradient $\partial/\partial x$ – see discussion by Kalliadasis *et al.* 2003). This is a realistic limit for liquids like water ($\gamma = 3000$), alcohols ($\gamma = 100$–300) and mercury ($\gamma = 30000$) – see for example Reid *et al.* (1977). Alternatively, the case $We\,Re \gg 1$ can also be satisfied in microgravity conditions where the effective gravity is small.

With $We\,Re \sim \epsilon^{-2} \sim \alpha_0^{-2}$, the term $We\,Re\hat{h}_{xxx}$ in (15) is of $O(\alpha_0 \hat{h})$ and hence dominates the neglected terms of $O(\hat{h}\hat{h}_x) = O(\hat{h}^2 \alpha_0)$ in this equation. The capillary force term in (18*a*) is of $O(\alpha_0^2 \hat{h})$. The instability term is also of $O(\alpha_0^2 \hat{h})$. So to balance the nonlinearity $\hat{h}\hat{h}_x$ with these two terms we must have $\hat{h} = O(\alpha_0)$. We can also obtain that the time-derivative term balances the nonlinearity, instability and dissipation terms on the long time scale $t \sim \alpha_0^{-2}$. Hence, all terms in (18*a*) are of $O(\alpha_0^3)$ with the exception of the dispersion term $Ma\,Peb\hat{h}_{xxx}$ which is of $O(\alpha_0^4)$ and hence must be neglected. Recall that we kept the term $Ma\,Peb\hat{h}_{xx}$ in (17) assuming that it is larger than terms of $O(\hat{h}\hat{h}_x)$: in fact $Ma\,Peb\hat{h}_{xx} \sim \hat{h}\hat{h}_x$ as indicated by the dominant terms in the weakly nonlinear equation (18*a*). Notice here that Pe cannot be large for our iterative scheme in (13*b*) to be valid.

As a result, the weakly nonlinear stage of the instability for strong capillary forces is governed by the KS equation and not the Kawahara equation. Let us now consider the possibility $Re - Re^* \to 0$ and c_3 fixed, say $O(1)$. This implies that $We\,Re$ is also $O(1)$ which of course violates the basic assumption of strong capillary forces for the IBL derivation. Nevertheless, the question of whether or not Kawahara's equation is applicable at the weakly nonlinear stage of the instability within the context of our IBL model is still relevant.

With $c_3 = O(1)$ and $Re - Re = (\alpha_0^2)$ (as is obviously the case from the dispersion relation in (10*a*)) both the capillary-force term and the instability terms in (18*a*) are of $O(\alpha_0^4 \hat{h})$. To balance the quadratic nonlinearity with these two terms we must have $\hat{h} = O(\alpha_0^3)$. Therefore, the term $We\,Re\hat{h}_{xxx}$ in (15) is of $O(\alpha_0^6)$ and hence dominates the neglected terms of $O(\hat{h}\hat{h}_x) = O(\alpha_0^7)$. The time-derivative term also balances the nonlinearity, instability and dissipation on the long time scale $t \sim \alpha_0^{-4}$. Hence, all terms in (18*a*) are of $O(\alpha_0^7)$ with the exception of the dispersion term which is of $O(\alpha_0^6)$! As a result, to obtain Kawahara's equation from our IBL approximation we must have $Pe = O(\alpha_0)$. This implies that $Ma\,Peb\hat{h}_{xx}$ in (17) is of $O(\alpha_0^6)$ and hence dominates the neglected terms of $\hat{h}\hat{h}_x = O(\alpha_0^7)$ in this equation. Notice that the dispersion coefficient a_3 in the Kawahara equation (18a) changes sign at $Bi = 15/7 \simeq 2.1$

We can also derive (18a) from a 'rigorous' approach using the method of multiple scales. Let us take the case $Re - Re^* \to 0$ and $c_3 = O(1)$. We introduce slow variables $T_0 = t$, $T_1 = \alpha_0^n t$ and $X = \alpha_0 x$, so that

$$\frac{\partial}{\partial t} = \frac{\partial}{\partial T_0} + \alpha_0^n \frac{\partial}{\partial T_1}, \quad \frac{\partial}{\partial x} = \alpha_0 \frac{\partial}{\partial X} \tag{19a}$$

and expand the unknown film thickness, flow rate and free-surface temperature field as

$$h \sim 1 + \alpha_0^m H(T_0, T_1, X), \tag{19b}$$

$$q \sim 1 + \alpha_0^k Q(T_0, T_1, X), \tag{19c}$$

$$T_s \sim -1 + \alpha_0^\ell \Theta(T_0, T_1, X). \tag{19d}$$

We also assume that $Pe = O(\alpha_0)$. Substituting (19) into the full (one-dimensional) system (2a–c), (4) we obtain as a first approximation, $\partial H/\partial T_0 + 3\partial H/\partial X = 0$, and hence, to leading order, the waves do not have dispersion, dissipation or supply of energy. We substitute $\partial/\partial T_0 = -3\partial/\partial X$ in (19) (this is equivalent to considering from the outset our equations in a reference frame moving with the long-wave linear phase velocity 3) and examine the next approximation. At this stage we keep only terms quadratic in H and we try to balance the dominant nonlinear term HH_X with the other terms. This algebraic exercise is rather tedious and we only present the order assignments of each term in (19) relative to α_0. To balance nonlinearity, dispersion and supply of energy, the proper choice for the expansion ansatz in (19) is $n = 4$ and $m = k = \ell = 3$. These exponents are consistent with the order of magnitude assignments $t \sim \alpha_0^{-4}$ and $\hat{h} \sim \alpha_0^3$ to obtain the Kawahara equation (18a) using the iterative procedure we described above. The final result is exactly (18a). A similar methodology can be used when $c_3 \gg 1$ and $Re - Re^* = O(1)$. In this case, $n = 2$ and $m = k = \ell = 1$.

All the above derivations presuppose the orders of the parameters and retain only the relevant terms at each order of the long-wave expansion. Notice that the values for the exponents in (19) are such that Q and Θ can be eliminated, resulting in a single equation for H in the weakly nonlinear stage of the instability. This elimination is due to the fact that two of the roots of the dispersion relation in (9) are stable. A different approach has been suggested by Whitham (1973): the linearized version of the model equation at the weakly nonlinear stage of the instability can be readily obtained by noticing that there is a direct correspondence between the dispersion relation in (10) and the linearized differential operator of this model equation. For example the terms $-\mathrm{i}\omega \equiv -\mathrm{i}\alpha c$ and $\mathrm{i}\alpha$ of the dispersion relation should correspond to the derivatives $\partial/\partial t$ and $\partial/\partial x$ of the model equation respectively. The same approach was adopted by Nepomnyashchy *et al.* (2002). However, we have three variables, h, q and T_s, and hence our linearized operator of the model equation should be a matrix/differential operator so that the model equation will in general be different from (18a) which is a single equation for $\hat{h}$ since q and T_s have been adiabatically eliminated (recall that as a result of this elimination the dispersion relation of the reduced model equation has only one root instead of three). In the particular case, however, when $Re - Re^* \to 0$ and $c_3 \gg 1$ we can write down a single equation for $\hat{h}$

using Whitham's approach. From the expansion for the phase velocity in (10),

$$\frac{\partial \hat{h}}{\partial t} + 3\frac{\partial \hat{h}}{\partial x} + c_1\frac{\partial^2 \hat{h}}{\partial x^2} - c_2\frac{\partial^3 \hat{h}}{\partial x^3} - c_3\frac{\partial^4 \hat{h}}{\partial x^4} = 0,$$

since $c_1 = a_1$, $c_2 = -a_3 + O(Re - Re^*)$ and $c_3 \sim -a_2$. This equation in a frame of reference moving with velocity 3 is the linearized version of (18*a*).

Finally, notice that the transformation

$$t \to \sqrt{\tfrac{2}{3}}a_1^{-5/4}a_2^{3/4}t, \quad x \to \sqrt{\frac{a_2}{a_1}}x, \quad \hat{h} \to \sqrt{\tfrac{2}{3}}a_1^{3/4}a_2^{-1/4}\hat{h}$$

converts (18*a*) into

$$\frac{\partial \hat{h}}{\partial t} + 6\hat{h}\frac{\partial \hat{h}}{\partial x} + \frac{\partial^2 \hat{h}}{\partial x^2} + \frac{\partial^4 \hat{h}}{\partial x^4} + \Delta\frac{\partial^3 \hat{h}}{\partial x^3} = 0$$

which contains the single parameter $\Delta = \sqrt{2/3}a_3a_1^{1/4}a_2^{-1/4}$. In the limit $\Delta \to 0$, our model equation is free of parameters.

4.2. *The Joo, Davis & Bankoff equation*

The equation developed by Joo *et al.* (1991) (subsequently referred to as the JDB equation) was discussed in the Introduction. In the absence of evaporation effects/intermolecular forces and in terms of the variables and dimensionless groups adopted here their evolution equation for the film thickness can be written in the form

$$\frac{\partial h}{\partial t} + \frac{\partial q}{\partial x} = 0, \tag{20a}$$

$$q = h^3 + \frac{We\,Re}{3}h^3\frac{\partial^3 h}{\partial x^3} - \cot\theta h^3\frac{\partial h}{\partial x} + \frac{6}{5}Reh^6\frac{\partial h}{\partial x} - \frac{1}{2}Mah^2\frac{\partial}{\partial x}\left\{\frac{BiT_{\mathrm{air}}}{1+Bih}h\right\}. \tag{20b}$$

An equation very similar to the JDB equation (20) can be derived from the one-dimensional version of our IBL approximation in (2*a*–*c*), (4). Here we follow the approach developed by Ruyer-Quil & Manneville (1998) to obtain a Benney-type evolution equation from the IBL approximation for the isothermal falling film. The approach is similar to the procedure outlined in §4.1. Let us assume that both the interface temperature T_s and the flow rate q are adiabatically slaved to the film thickness h and depend on time only through the dependence of h on time. As a first approximation set all derivatives in (2*a*), (4) equal to zero to obtain (12*a*, *b*). These expressions for the flow rate and interface temperature are exact solutions for the problem, provided that the free-surface gradient is small. When this is no longer the case corrections have to be introduced. For this purpose we consider slow modulations to the uniform flat-film solution and expand the flow rate and interface temperature as $q = q_0 + q_1 + \cdots$, $T_s = T_{s0} + T_{s1} + \cdots$ where $q_0 \equiv h^3$, $T_{s0} = BiT_{\mathrm{air}}h/(1 + Bih)$ and $q_{1,2,\ldots}$, $T_{s1,2,\ldots}$ are $O(\epsilon)$, $O(\epsilon^2)$ etc. with respect to the long-wave parameter ϵ that measures the gradient $\partial/\partial x$. These expansions are then substituted into the one-dimensional version of (2*a*), (4) and we retain terms up to $O(\epsilon)$ in (2*a*) and up to $O(1)$ in (4). For example, $\partial q_0/\partial t = 3h^2\partial h/\partial t = 3h^2(-\partial q_0/\partial x - \partial q_1/\partial x - \cdots) \sim -3h^3\partial q_0/\partial x = -9h^4\partial h\partial x = O(\epsilon)$. The result is

$$q_1 = \frac{We\,Re}{3}h^3\frac{\partial^3 h}{\partial x^3} - \cot\theta h^3\frac{\partial h}{\partial x} + Reh^6\frac{\partial h}{\partial x} - \frac{1}{2}Mah^2\frac{\partial}{\partial x}\left\{\frac{BiT_{\mathrm{air}}}{1+Bih}h\right\}$$

where the capillary force and Marangoni terms are taken to be $O(\epsilon)$ with $We\,Re = O(\epsilon^{-2})$ and $Ma = O(1)$.

This approach can be easily formulated in an iterative scheme to obtain the higher-order corrections for the flow rate and interface temperature. The evolution equation is then obtained from $\partial h/\partial t + \partial(q_0 + q_1)/\partial x = 0$ up to $O(\epsilon)$ which leads to an equation very similar to the JDB model except that the coefficient of the inertia term is 1 instead of 6/5. This difference is simply due to the assumption of a self-similar parabolic profile for IBL. Recall from the previous Section that this assumption leads to estimating critical conditions with a 20% error compared to the Orr–Sommerfeld stability analysis of the full Navier–Stokes equation and the usual long-wave lubrication approximation. Indeed, the dispersion relation obtained from the JDB model in (20) is

$$c = 3 - \mathrm{i}\alpha^3 \frac{We\,Re}{3} + \mathrm{i}\alpha\left(\frac{6}{5}Re - \cot\theta\right) + \frac{1}{2}\mathrm{i}\alpha\frac{Ma}{1+Bi} \tag{21}$$

which yields the critical condition

$$\frac{6}{5}Re + \frac{Ma}{2(1+Bi)} = \cot\theta \tag{22}$$

with a 6/5 coefficient in front of Re instead of 1 in (11a) obtained from IBL. As a result, when (22) is written in terms of the dimensionless groups χ, B and M, it is exactly the same as the critical condition obtained by Goussis & Kelly with coefficients 15/16 and 5/4 in (11b) instead of 9/8 and 3/2. The agreement with the full Navier–Stokes equation persists up an $O(1)$ value of the Reynolds number – see the comparison of the long-wave approximation in the presence of thermocapillary effects with the full Navier–Stokes equation performed by Krishnamoorthy, Ramaswamy & Joo (1995) and Ramaswamy, Krishnamoorthy & Joo (1997). However, by analogy with the long-wave approximation in the absence of thermocapillary effects, we anticipate that the Benney-type JDB equation (20) will have similar limitations. We shall return to this point in § 5 when we compare the solitary wave solutions of the IBL and JDB approximations. Notice here, that like the KS equation derived in § 4.1, the JDB dispersion relation in (21) predicts only one mode. Hence neither approach captures the upstream propagating surface mode and Marangoni mode obtained from the IBL dispersion relation in (9).

A point to be noted here is that a temperature field adiabatically slaved to the film thickness has often been used in the literature (Joo *et al.* 1991; Burelbach, Bankoff & Davis 1988; Bankoff 1994; Oron 1999; Oron & Peles 1998; Scheid *et al.* 2001). This is a consequence of the long-wave approximation for the temperature adopted by these authors. Obviously, the temperature field is indeed slaved to the thickness when $Pe \ll 1$. In this limit, convection is negligible compared to heat diffusion and the interface temperature is simply given by T_{s0}. If we further assume that $Re \ll 1$, IBL and the JDB model are identical. Hence, the usual long-wave expansion is a limiting case of IBL for $Re = Pe = 0$. However, it is very difficult to achieve $Pe = 0$ in practice; for example in the experiments by Kabov (1998) on the thermocapillary instability of a thin liquid film falling down a vertical substrate heated by a local heat source, the Péclet number is $O(1)$ or even larger. Clearly, convection at finite Péclet numbers will lead to a downstream convective distortion of the surface temperature profile T_{s0} which assumes negligible convection. Alternatively, the temperature field is slaved to the film thickness when the deviation of the film thickness from 1 is small. This implies that the region of applicability of the JDB equation is effectively the same as that of KS equation obtained in § 4.1 and hence Benney-type model equations are essentially restricted to small amplitudes and cannot describe finite-amplitude waves as is often claimed in the literature.

4.3. *Model equation for strong Marangoni forces, $\chi \to 0$*

In the linear stability analysis of § 3, we demonstrated that for small Reynolds numbers the influence of the Marangoni effect is sufficiently strong that the maximum growth rate of the downstream propagating mode is large. In fact, it increases as the Reynolds number (or χ) decreases. Let us consider the case $\chi \to 0$ (not to be confused with the case $a_1 = Re - Re^* \to 0$ utilized in § 4.1 to obtain the KS equation) which can be achieved with $h_0 \to 0$.

For small Reynolds numbers, it is reasonable to assume that the flow rate is slaved to the film thickness. An approach similar to that outlined in §§ 4.1 and 4.2 then yields

$$q = h^3 - \cot\theta h^3 \frac{\partial h}{\partial x} + \frac{We\,Re}{3} h^3 \frac{\partial^3 h}{\partial x^3} - \frac{1}{2} Ma h^2 \frac{\partial T_s}{\partial x}. \tag{23a}$$

The interface temperature field may or may not be slaved to the film thickness. This depends on the size of the Péclet number. Since $Pe = Re\,Pr$, for a given fluid Pr is fixed and we cannot really vary Re and Pe independently. In this case, $Re \to 0$, implies $Pe \to 0$ and T_s is given by (12*b*). But $Bi = B\chi^{1/3} \to 0$ so that

$$T_s = -h \tag{23b}$$

and our evolution equation in this limit becomes

$$\frac{\partial h}{\partial t} + \frac{\partial}{\partial x}\left[h^3 - \cot\theta h^3 \frac{\partial h}{\partial x} + \frac{We\,Re}{3} h^3 \frac{\partial^3 h}{\partial x^3} + \frac{1}{2} Ma h^2 \frac{\partial h}{\partial x}\right] = 0. \tag{24}$$

As we pointed out in § 4.2, in the limit $Re = Pe = 0$, the JDB and IBL approximations are identical.

Consider now the coefficients of the capillary force and Marangoni terms in (24). From the definitions of We and Ma in (1*b*, *d*)

$$\frac{We\,Re}{3} = \frac{\gamma}{3^{2/3} Re^{2/3} (\sin\theta)^{1/3}},$$
$$\frac{1}{2} Ma = \frac{1}{2} \frac{3M}{18^{1/3} Re^{2/3} (\sin\theta)^{1/3}}.$$

Hence, for a fixed liquid and as $\chi \to 0$, both capillary and Marangoni forces scale as $\chi^{-2/3}$. Interestingly, for a falling film in the absence of Marangoni effects, the destabilizing inertia terms are vanishing in the limit $\chi \to 0$. In our case, the destabilizing terms are surface forces and are still present as $\chi \to 0$. The stabilizing terms are also surface forces with the same dependence on χ. As a result, the cut-off wavenumber α_0 above which the linear growth rate of the trivial solution $h = 1$ becomes negative is independent of χ. These observations are also consistent with the existence of a finite α_0 at which the neutral stability curve in figure 3(*a*) intersects the α-axis as $\chi \to 0$. We note that from a physical point of view, the term h^3 in (24) associated with the gravitational component in the streamwise direction is a 'friction force' while the term $-\cot\theta h^3 h_x$ in (24) associated with the hydrostatic head in the direction perpendicular to the wall is a 'spring force' and hence is not responsible for the instability – in fact a linear stability analysis of the trivial solution $h = 1$ in (24) shows that $-\cot\theta h^3 h_x$ is always stabilizing. For large inclination angles this term can be safely omitted. In this limit, saturation of the linear growth must involve a balance of the nonlinear convective term $(h^3)_x$ and the two surface-force terms in (24). One can render this balance more precise by rescaling time and spatial coordinates according to

$$\frac{\partial}{\partial t} = \phi \frac{\partial}{\partial \tau}, \quad \frac{\partial}{\partial x} = \phi \frac{\partial}{\partial \xi},$$

and choosing ϕ so that the coefficients of the Marangoni and capillary forces in (24) are equal:

$$\phi = \frac{3^{5/6} M^{1/2}}{2^{1/2}(18)^{1/6} \gamma^{1/2}}. \tag{25a}$$

This yields the nonlinear evolution equation

$$\frac{\partial h}{\partial \tau} + \frac{\partial}{\partial \xi}\left[h^3 + \frac{1}{\delta} h^3 \frac{\partial^3 h}{\partial \xi^3} + \frac{1}{\delta} h^2 \frac{\partial h}{\partial \xi}\right] = 0 \tag{25b}$$

which contains the single parameter

$$\delta = \frac{4\gamma^{1/2}}{3^{5/6} M^{3/2}} Re^{2/3} (\sin\theta)^{1/3}. \tag{25c}$$

Hence, in the limit of $\chi \to 0$ and for large inclination angles, the behaviour of the interface depends on δ only and it is universal for all Re, M and γ.

5. Solitary waves

We now seek one-dimensional travelling wave solutions propagating at a constant speed c. A Lagrangian transformation of the one-dimensional mass balance equation in (2c) with $x \to x - ct$ and $\partial/\partial t = -c\partial/\partial x$ in the moving frame then yields $-ch_x + q_x = 0$ which can be integrated once, and we fix the integration constant by demanding $h, q \to 1$ as $x \to \pm\infty$. This gives a relation between the flow rate and the film thickness:

$$q = c(h-1) + 1. \tag{26}$$

We also introduce the moving coordinate transformation in the one-dimensional versions of (2a) and (4), which by utilizing (26) yield

$$-c^2 \frac{\mathrm{d}h}{\mathrm{d}x} + \frac{6}{5}\frac{\mathrm{d}}{\mathrm{d}x}\left\{\frac{[c(h-1)+1]^2}{h}\right\} + \frac{3}{2}\frac{\cot\theta}{Re} h \frac{\mathrm{d}h}{dx} = Weh\frac{\mathrm{d}^3 h}{\mathrm{d}x^3} + \frac{3}{Re}\frac{(h-1)(h^2+h+1-c)}{h^2} - \frac{3}{2} Ma \frac{\mathrm{d}T_s}{\mathrm{d}x} \tag{27}$$

and

$$-c\frac{\mathrm{d}T_s}{\mathrm{d}x} + \frac{7}{40}\frac{T_s}{h} c \frac{\mathrm{d}h}{\mathrm{d}x} + \frac{27}{20}\frac{(c-1)h+1}{h}\frac{\mathrm{d}T_s}{\mathrm{d}x} + \frac{3}{Pe}\left\{\frac{Bi(T_s - T_{\mathrm{air}})}{h} + \frac{T_s}{h^2}\right\} = 0, \tag{28}$$

where $T_{\mathrm{air}} = -(1+Bi)/Bi$. These equations, together with the boundary conditions

$$h \to 1, \quad T_s \to -1 \quad \text{as} \quad x \to \pm\infty, \tag{29}$$

with all the derivatives of both h and T_s approaching zero as $x \to \pm\infty$, define a nonlinear eigenvalue problem for the solitary wave velocity c. The solitary wave solutions of our IBL approximation will be contrasted with the solitary waves obtained

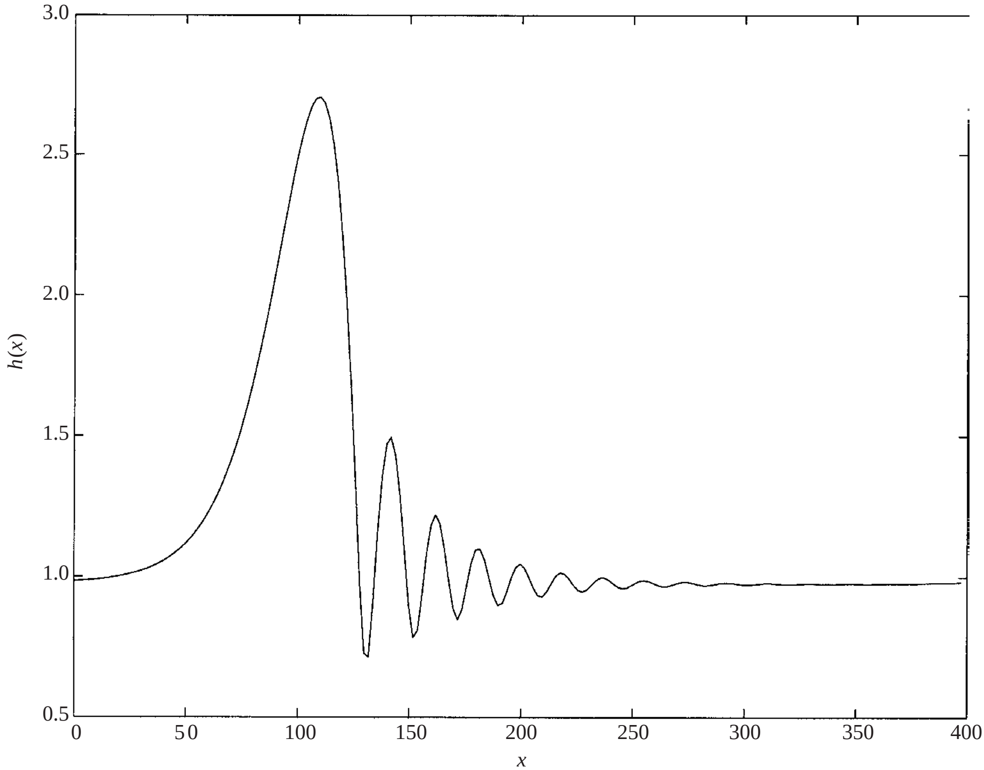

FIGURE 5. Solitary pulse in an extended domain for $\chi = 7.5$, $M = 75$, $Pr = 1$, $B = 10$ and $\gamma = 3000$.

from the JDB equation (20) which in the moving frame can be written as

$$\frac{\mathrm{d}}{\mathrm{d}x}\left[-\frac{18}{25}h^5 + \frac{3\cot\theta}{Re}h^2\right] = Weh\frac{\mathrm{d}^3h}{\mathrm{d}x^3} + \frac{3}{Re}\frac{(h-1)(h^2+h+1-c)}{h^2} - \frac{3}{2}\frac{Ma}{Re}\frac{\mathrm{d}T_s}{\mathrm{d}x} \tag{30}$$

subject to $h(\pm\infty) = 1$. T_s is slaved to the film thickness and is given by

$$T_s = \frac{BiT_{\mathrm{air}}}{1+Bih}h. \tag{31}$$

We solve numerically the IBL system (27), (28) and the JDB equation (30) with a global Fourier spectral expansion in the streamwise coordinate x. Details of the numerical scheme are given by Bunov, Demekhin & Shkadov (1984), Chang, Demekhin & Kopelevich (1993*b*) and Kalliadasis *et al.* (2003).

In all our computations we take $\theta = \pi/2$ and the maximum value of the Reynolds number does not exceed 20. In fact, when the Reynolds number is larger than $\sim$30–40, two-dimensional solitary waves become unstable to disturbances in the transverse direction (Alekseenko *et al.* 1994). In this region of 'large' Reynolds numbers, the stabilizing capillary forces are not strong enough to arrest the large destabilizing inertia forces and an instability in the transverse direction develops. Figure 5 shows a typical solitary pulse in an extended domain for the 'moderate' value $\chi = 7.5$ (which gives $Re = 5$) and the large value $M = 75$, with $Pr = 1$, $B = 10$ and $\gamma = 3000$ (water has $\gamma = 3000$ but $Pr = 7$). Here we shall focus on single-hump solitary waves. Notice that the wave has a width $\sim$100 and an amplitude $\sim$2 such that our long-wave assumption

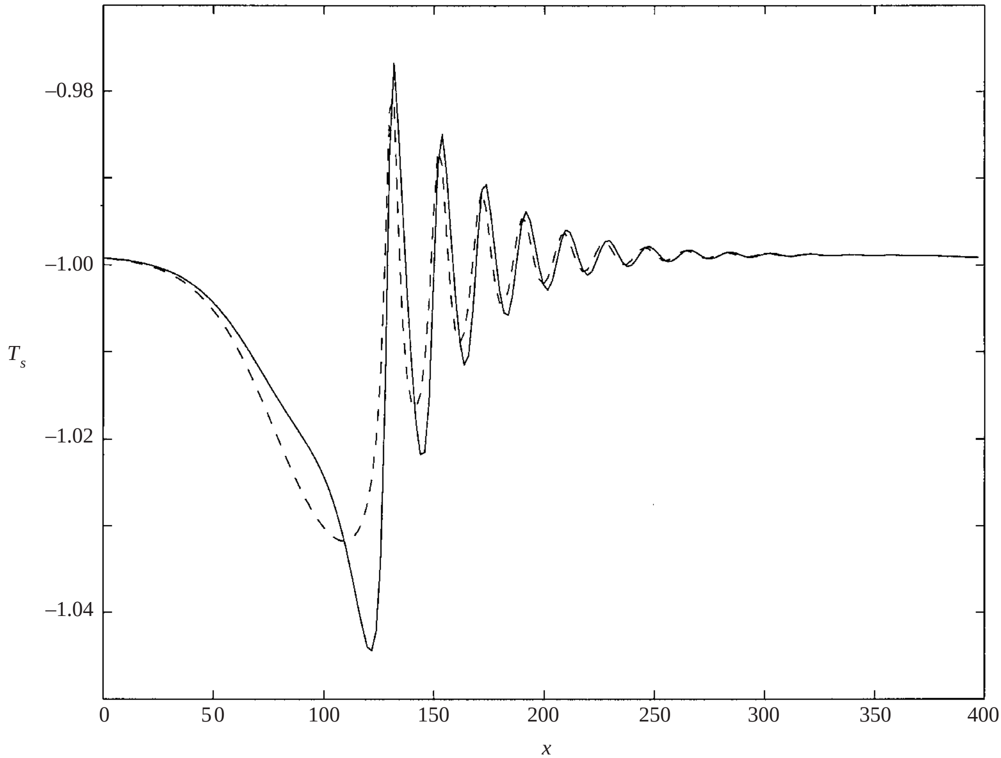

FIGURE 6. Interface temperature distribution for the parameter values in figure 5. The solid line is obtained by solving the system (27), (28) and the dashed line by solving (27) with the temperature field given by (31).

is satisfied. The shape of the solitary pulse in figure 5 is qualitatively similar to the solitary pulses computed for the falling film in the absence of Marangoni effects. This 'generic' solitary wave shape consists of a big hump with a gentle sloping back edge and a steep front edge preceded by a series of small, decaying bow waves. This oscillatory structure in front of a solitary pulse is due to energy dissipation (on short wavelengths). For the Kawahara equation (dissipation is represented by a fourth-order derivative), Kawahara & Toh (1988) demonstrated that increasing dissipation leads to enhanced oscillatory structure in front of the pulses. A detailed characterization of our solitary pulses using techniques from dynamical systems theory (see for example Nekorkin & Velarde 1994) is beyond the scope of the present study; nevertheless we anticipate that the solitary pulse in figure 5 corresponds to a homoclinic orbit of the dynamical system (27), (28) with a large loop followed by damped oscillations toward the fixed point connected to the loop. Note that since the front-running capillary waves correspond to the local dynamics near the fixed point $(h, T_s) = (1, -1)$, a simple linear analysis shows that the bow waves have a wavenumber close to the neutral wavenumber α_0.

Figure 6 depicts the interface temperature distribution for the parameter values in figure 5. The solid line is obtained by solving the system (27), (28) and the dashed line by solving (27) with T_s slaved to the film thickness and given by (31). The system (27), (31) is obviously different from the JDB model in (30), (31) where both flow rate and temperature fields are slaved to the film thickness. Clearly, for $Pr = 1$, the two systems give a similar temperature distribution. Notice that T_s is also a solitary pulse

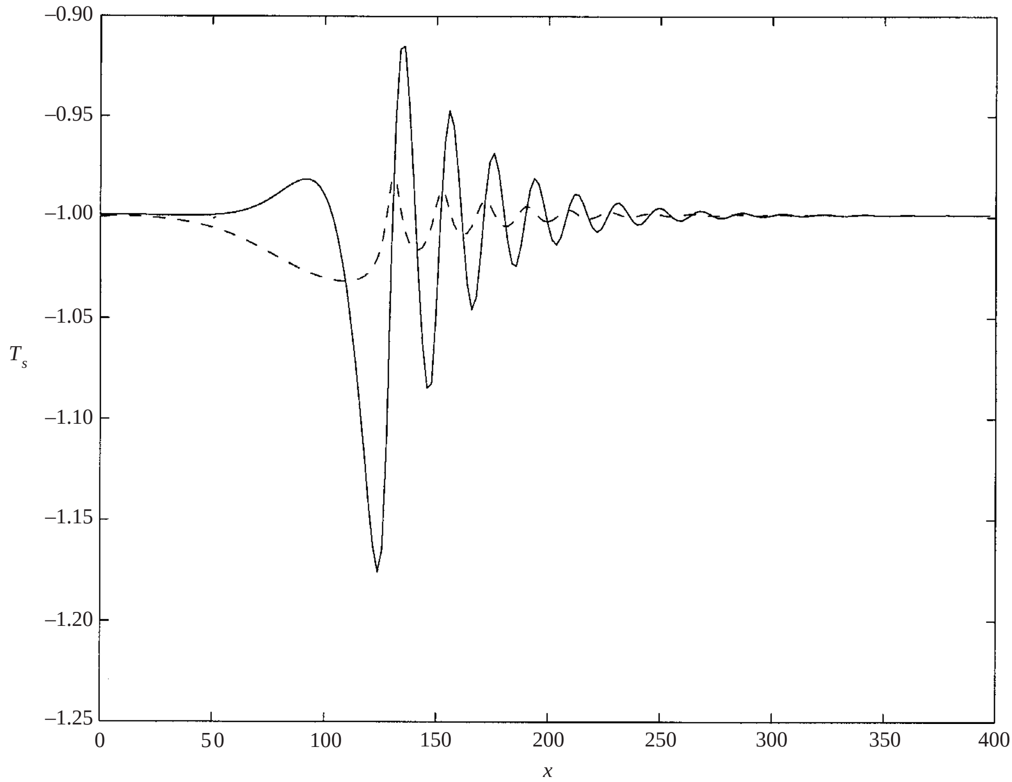

FIGURE 7. Interface temperature distribution for $Pr = 7$. All other parameter values are the same as figure 5. The solid line is obtained from (27), (28) and the dashed line from (27), (31).

with a shape similar to the interface configuration in figure 5. figure 7 shows the free-surface temperature distributions for $Pr = 7$. Notice that the temperature distribution obtained from (31) (dashed line in figures 6 and 7) is slaved to the film thickness and hence is independent of Pr. The free surface itself is not shown as the solitary wave shape of Figure 5 remains practically the same for the range of Pr values considered here. This is simply due to the fact that for moderate χ the influence of Marangoni effects (and therefore the influence of the temperature field on the instability), is small (see § 3).

Evidently, on increasing the Prandtl number, the difference between the two temperature profiles becomes more pronounced and the approach of T_s slaved to h gives an erroneous prediction for the temperature field. The difference between the two approaches is due to the fact that the energy flux in the full IBL model of (28) has two components, diffusion and convection, instead of diffusion only for the slaved profile in (31). For long waves, convection is dominated by $\partial(vT)/\partial y$ and indeed our computations show that this term is very important. Of course for long waves v is small, but as the Prandtl number increases (equivalently as Pe increases) the convective term $\partial(vT)/\partial y$ in the energy equation becomes large and increases the heat flux in the y-direction. For the slaved profile in (31), however, the heat flux is only due to the diffusion term $(1/Pe)\partial^2 T/\partial y^2$.

Figures 6 and 7 also demonstrate that increasing Pr and hence Pe increases the amplitude of the bow waves at the front of the primary hump for the temperature

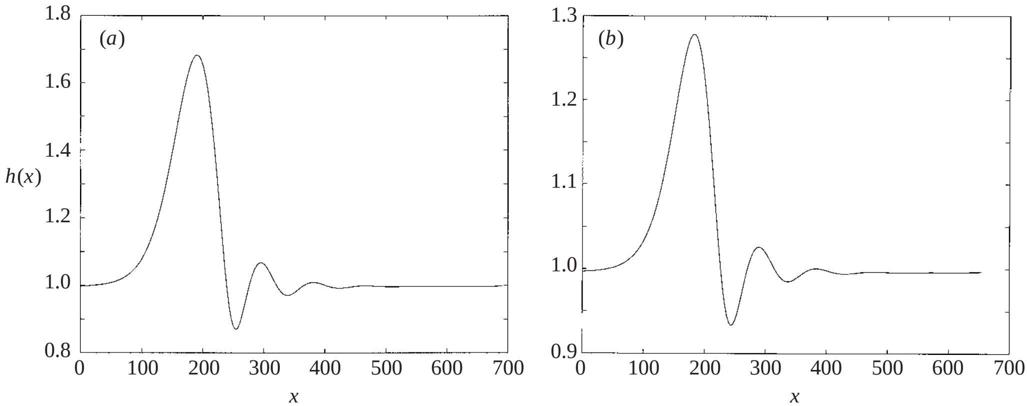

FIGURE 8. (*a*) Free-surface solitary wave for $Pr = 1$, $\chi = 0.15$. (*b*) free-surface solitary wave for $Pr = 7$, $\chi = 0.45$; $M = 75$, $B = 10$ and $\gamma = 3000$.

pulse. This is simply due to the fact that increasing *Pe* increases energy dissipation. Notice that for the slaved temperature pulse, the maximum amplitude of the bow waves at the front of the pulse is rather large compared to the amplitude of the pulse. This might imply that the temperature pulse is not stable and will be destroyed in time-dependent numerical experiments. Such experiments along with issues related to convective instabilities of solitary pulses are beyond the scope of the present study – see the work of Chang *et al.* (1995) on the destruction of solitary pulses of Kawahara's equation by expanding radiation packets and the study by Kliakhandler, Porubov & Velarde (2000) on the solitary wave selection process from a given initial condition for the Korteweg–de Vries–KS–Velarde equation.

Figure 8(*a*) shows a free-surface solitary wave for $Pr = 1$, $\chi = 0.75$ and $M = 75$ while figure 8(*b*) shows a free-surface solitary wave for $Pr = 7$, $M = 75$ and the $O(1)$ value, $\chi = 0.45$. For small to $O(1)$ values of χ, dissipation is gentle and the bow waves at the front of the primary solitary hump have a much smaller amplitude than the maximum amplitude of the hump – contrast with figure 5 where χ and therefore energy dissipation are large. Hence, the solitary structures in figure 8 are likely to be more robust in time-dependent computations than the one in figure 5.

The maximum amplitude of the solitary wave in figure 5 is larger than the maximum amplitude of the solitary wave in figure 8 even though χ in figure 8 is smaller than χ in figure 5. This is because the influence of the Marangoni effect on the hydrodynamics becomes large in the region of very small χ (see § 3). In fact, we shall demonstrate that in this region, the maximum amplitude of the solitary waves increases as χ decreases. Notice also that even though the amplitude in figure 8 is smaller than that in figure 5, relative to the flat-film thickness the free-surface deformation in figure 8 is larger than that in figure 5; indeed, the solitary wave amplitude is reduced from about 2.7 in figure 5 to about 1.7 and 1.3 in figure 8 but the film thickness is reduced by a factor of $(7.5/0.15)^{1/3} \approx 3.7$ and $(7.5/0.45)^{1/3} \approx 2.6$ respectively. This is because the role of free-surface deformation is important in the region of small χ.

Figure 9(*a*) shows the free-surface temperature distribution for $Pr = 7$, $\chi = 0.15$ and $M = 75$. Despite this value of *Pr*, the Péclet number is sufficiently small that the temperature distribution is a weak function of *Pr* when *Pr* changes from 1 to 7. Hence, the profile obtained for $Pr = 7$ is almost identical to the one computed for $Pr = 1$. At the same time, small *Pe* implies small dissipation and so the oscillatory structure

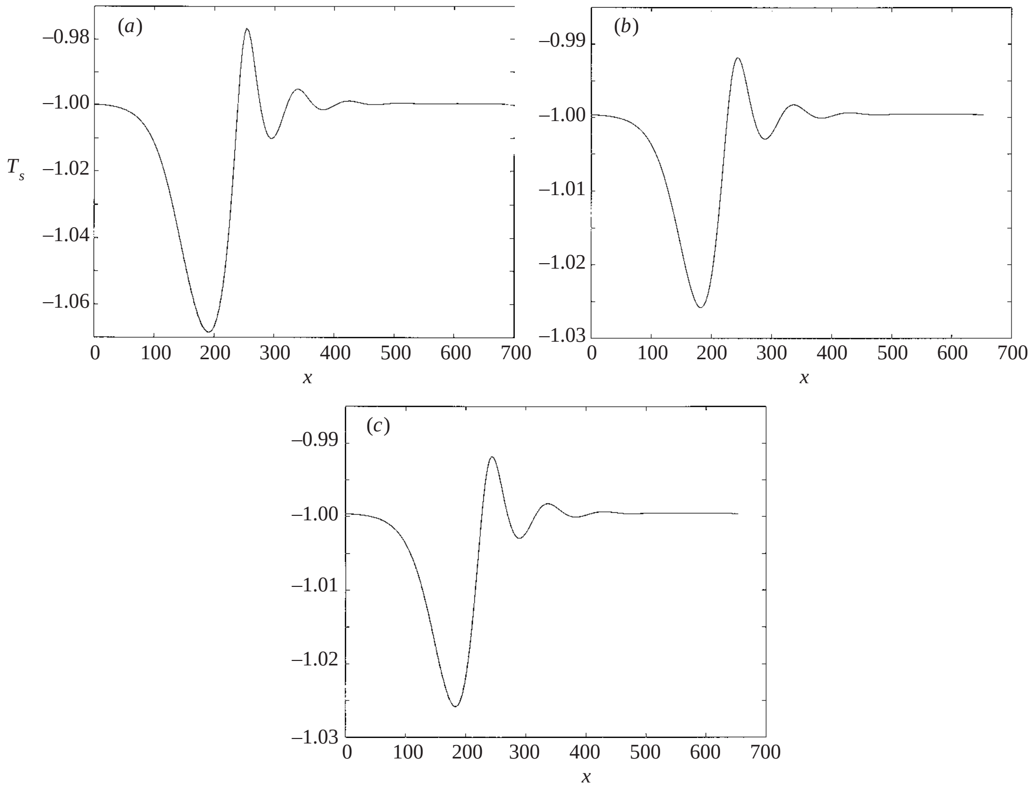

FIGURE 9. Interface temperature distributions for small and $O(1)$ values of χ. Solid lines obtained from (27), (28) and dashed lines from (27), (31) are practically indistinguishable: (a) $Pr = 7$ and all other parameter values are the same as figure 8(a)/(b) $Pr = 1$ and all other parameter values are the same as figure 8(b)/(c) parameter values as in figure 8(b).

in front of the primary hump for the temperature solitary wave has a maximum amplitude much smaller than that of the primary hump. Therefore, we expect that such temperature profiles are robust in time-dependent numerical experiments. Notice that the two temperature distributions, slaved and not slaved (the solid line is obtained from (27), (28) and the dashed line from (27), (31)) are practically indistinguishable in the region of small χ, even for the 'large' value $Pr = 7$. The difference between the two profiles decreases further as Pr decreases.

In figures 9(b, c) we give the temperature distribution for different values of Pr with all other parameters the same as in figure (8b). In all cases, the two temperature distributions, slaved and not slaved, are practically indistinguishable and hence the assumption of a slaved temperature distribution is valid in the region of small to $O(1)$ values of χ. Notice also that increasing χ reduces the amplitude of the bow waves relative to the maximum amplitude of the primary solitary humps, as expected.

We now examine in detail important features of our solitary waves, namely their speed c and maximum amplitude $h_{\max}$. In figures 10 and 11 the solution branches obtained from the full IBL system (27), (28) as a function of χ for $Pr = 7$, $\gamma = 3000$ and different values of M, are contrasted with those obtained from the JDB system (30), (31) for the same values. We first discuss the IBL branches. The case $M = 0$ corresponds to a falling film without Marangoni effects. As $\chi \rightarrow 0$ both speed and maximum amplitude tend to infinity. This is the 'interesting' behaviour we referred

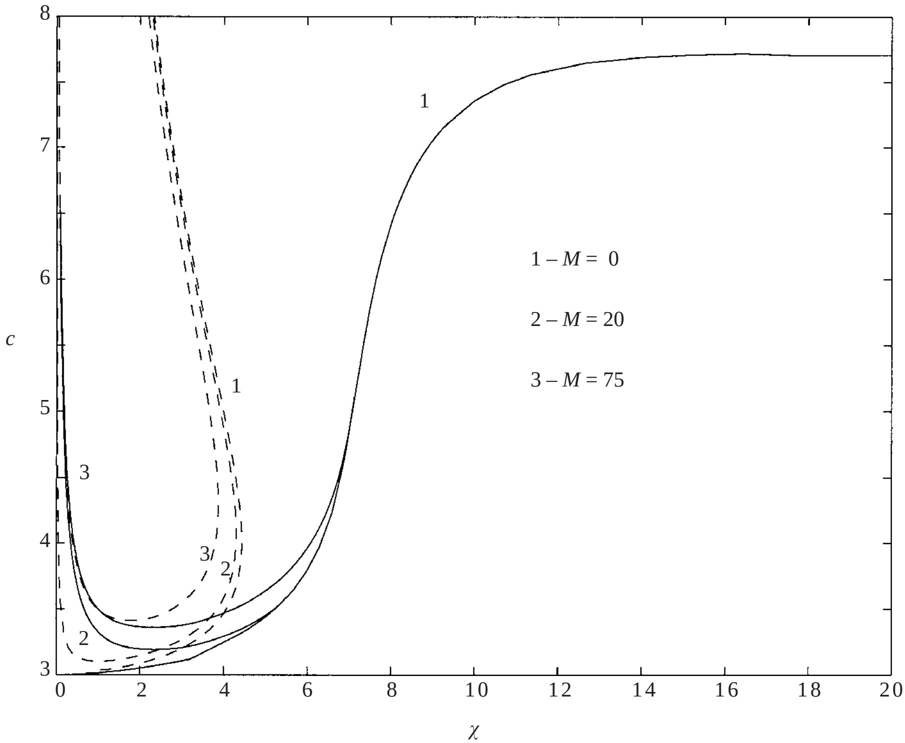

FIGURE 10. Solitary wave speed, c, as a function of χ for $B=10$, $Pr=7$, $\gamma=3000$ and different values of M. The solid lines correspond to the IBL model and the dashed line to the JDB model in (30), (31).

to in §3 where we demonstrated the existence of a finite α_0 as $\chi \to 0$ for $M \neq 0$ so that the influence of thermocapillary convection on hydrodynamics becomes large for small χ (very thin films) – see also the large growth rate of the unstable mode in figure 4(a). The region $\chi \to 0$ is of particular interest as in this limit the role of deformation is large and we expect large-amplitude waves relative to the flat film thickness. Notice that at a sufficiently large χ the different M curves in figures 10 and 11 merge into a single curve which eventually asymptotes to $c \approx 7.7$ and $h_{max} \approx 3.6$ for large χ. In this region of large χ and hence large film thickness, the surface Marangoni forces are not important compared to the dominant inertia forces. The only case when there is no singularity at $\chi=0$ is $M=0$, i.e. in the absence of Marangoni forces; however at any small but finite M, we have $c, h_{max} \to \infty$ as $\chi \to 0$. Finally, our computations indicate that the dependence of c on M is practically linear in the region of large χ and is nonlinear for small χ.

We have also traced the solitary wave solution branch by using (27) with slaved temperature field given by (31). Interestingly, the full IBL system (27), (28) and the system (27), (31) give very similar results for the speed c and amplitude h_{max} of the solitary waves as a function of χ. However, the temperature field computed from the two approaches is different, with the difference becoming large for moderate and large χ – see figures 6 and 7. Nevertheless, for large χ, i.e. thick layers, the influence of the temperature field on hydrodynamics is negligible. On the other hand, for small χ, i.e. thin films, the convective terms of the energy equation are negligible since in this case $Pe \ll 1$ and the temperature field is given by (31).

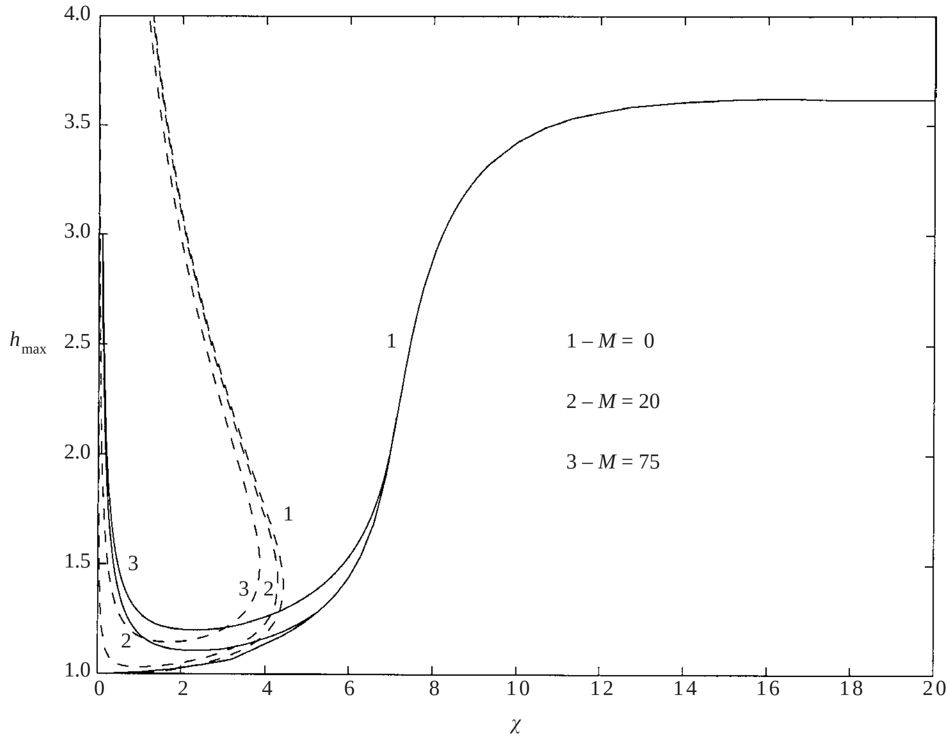

FIGURE 11. Maximum amplitude, h_{max}, of the solitary waves as a function of χ for different values of M. All other parameters are the same as figure 10. The solid lines correspond to the IBL model and the dashed lines to the JDB model (30), (31).

Let us now consider the JDB model where both flow rate and temperature field are adiabatically slaved to the film thickness. The most striking difference with IBL is that the bifurcation diagrams for c and h_{max} obtained from the JDB equation exhibit limit points and multiplicity with two branches, a lower branch and an upper branch. These limit points occur at specific values $\chi^*(M)$. In all cases the upper branch tends to infinity as $\chi \to 0$ while the lower branch tends to 3 for $M = 0$ and infinity for $M \neq 0$. This lower branch and for very small χ is in agreement with our IBL results; indeed, in this limit the JDB equation (20) reduces to the IBL equation (24). The agreement between the two approaches persists up to approximately χ^*, the location of the limit point, above which the JDB equation does not predict the existence of solitary waves. Hence, the situation is similar to the falling film problem in the absence of thermocapillary effects where the long-wave approximation and IBL give similar results up to an $O(1)$ value of χ. Our computations reveal that the existence of the upper branch for the JDB equation is due to the inertia term $(6/5)Reh^6h_x$. Hence, although this term yields the critical condition (22), which is exactly the same as the one obtained by Goussis & Kelly (1991), it also leads to branch multiplicity and limit points for the solitary wave solutions. This upper branch might well be an attractor in time-dependent computations, but such computations are beyond the scope of the present study.

The $M = 0$ curves were first computed by Pumir, Manneville & Pomeau (1983) who also demonstrated that the Benney-type evolution equation for the free surface exhibits finite-time blow-up behaviour for $\chi > \chi(0)$. Obviously, this unrealistic behaviour is related to the non-existence of stationary travelling waves in this region. As has been pointed out by several authors (see for example Rosenau, Oron & Hyman 1992), the limit points and branch multiplicity predicted by the usual long-wave approximation is a false prediction which indicates failure of the long-wave approximation. Of course none of these limitations are an issue in the region of very thin films where the Reynolds number is small and Benney's approach is exact, as we have already pointed out. At the same time, for $M = 0$, the region of applicability of the JDB model is the same as that of the KS equation, i.e. when h is close to 1 and the speed of the waves on the interface is close to 3. IBL, however, predicts the continued existence of travelling wave solutions without introducing any limiting χ values and for $M = 0$ the IBL solution branches are in quantitative agreement with the boundary-layer (Demekhin *et al.* 1987) and full Navier–Stokes equations for moderate Reynolds numbers (Demekhin & Kaplan 1989; Salamon *et al.* 1993; Ramaswamy *et al.* 1996). Finally, it should be noted that the differences between the bifurcation diagrams for the two approaches – recall that solving (27), (31) gives very similar results to (27), (28) – indicate that the assumption of a slaved flow rate, and not a slaved interface temperature field, is critical in accurately determining important features of the free-surface solitary waves such as speed and maximum amplitude (of course, the assumption of a slaved temperature distribution is not an accurate representation of the temperature field, as we have already emphasized).

We close this Section by examing in detail the solitary wave solutions for $\chi \to 0$. In this limit, our IBL approximation reduces to the model equation (25*b*). This equation is very similar to the equation used by Kalliadasis & Chang (1994) and by Chang & Demekhin (1999) to describe the evolution of a thin film coating a vertical fibre. Indeed, replacing the nonlinearity h^2 in (25*b*) with h^3 gives the evolution equation adopted by those authors. In terms of the scalings used by Kalliadasis & Chang, the coefficient of the axial curvature term $h^3 h_{\xi\xi\xi}$ is 1 while the coefficient of the term $h^3 h_\xi$ that describes the azimuthal curvature variation in the axial direction is $(Re\, We/3)^{2/3}/R^2$, with R the dimensionless fibre radius (scaled with the flat-film thickness h_0).

We now seek travelling wave solutions of (25*b*) in the form $h(\xi)$, with $\xi \to \xi - ct$, and c the wave speed. Introducing this moving coordinate transformation in (25*b*), integrating the resulting equation once, and fixing the integration constant by demanding $h \to 1$ as $\xi \to \pm\infty$, gives

$$h^3 \frac{\mathrm{d}^3 h}{\mathrm{d}\xi^3} + h^2 \frac{\mathrm{d}h}{\mathrm{d}\xi} + \delta[h^3 - 1 - c(h-1)] = 0. \qquad (32)$$

Figure 12 depicts (single-hump) solitary pulses as a function of δ with δ small. Clearly, with decreasing δ, both wave amplitude and width increase. From the definition of δ in (25*c*) we see that increasing M leads to decreasing δ which in turn results in increasing $h_{\max}$, as expected since large M has a large effect on the hydrodynamics. At the same time, increasing θ results in increasing δ and hence reducing $h_{\max}$, as expected since for large inclination angles the flow is dominated by the inertia forces. Similarly, increasing Re increases δ and hence $h_{\max}$, as expected. We notice here that the growth of c and $h_{\max}$ in figures 10 and 11 as $\chi \to 0$ is not a true blow up, as other forces which would arrest the singularity are present in the limit $\chi \to 0$. These are the long-range attractive van der Waals interactions between the solid and the gas phase separated by the liquid phase – these forces have been included in the study by Joo *et al.* (1991). Such interactions depend on an appropriately non-dimensionalized Hamaker's constant that would introduce a lower bound on the rate at which χ

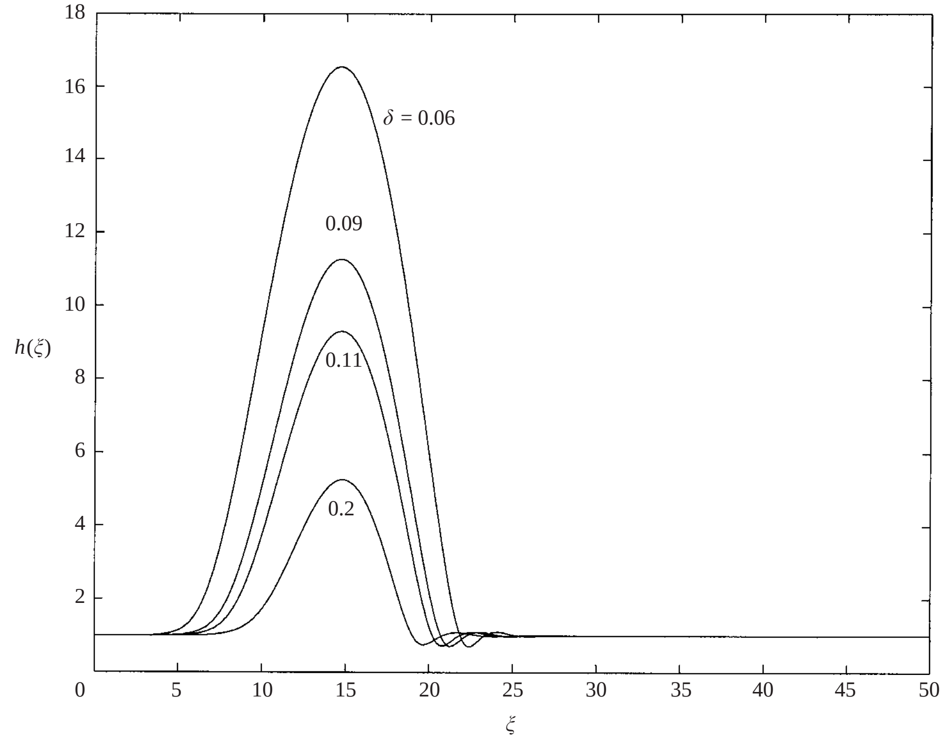

FIGURE 12. Solitary pulses for different values of δ, in the region $\delta \ll 1$, for the model equation (25*b*).

approaches zero. Nevertheless, the existence of large-amplitude structures in the region of small χ indicates that the system would approach a series of drops in time-dependent computations. Each of these drops should resemble a solitary wave for the free surface. Indeed standard techniques from dynamical systems theory show that in a neighbourhood of a solitary pulse in the parameter space there exists an entire family of stationary solutions, some of which are periodic in x, with speeds c close to the solitary wave speed. A periodic wave generated by an (infinite) solitary pulse resembles a solitary periodic wavetrain with each of the structures in the train similar to the infinite-domain solitary pulse. In time-dependent computations the dynamics of the drop-formation process might include phenomena related to coalescence between smaller and larger waves – we shall discuss this point later. Of course, the final state of the system depends on the wetting characteristics of the liquid–solid pair. Indeed, completely wetting fluids should form a series of drops separated by a very thin flat film (such a film can only be sustained when the liquid is completely wetting) and partially wetting fluids should form a series of drops separated by dry solid substrate – in this case the van der Waals interactions will cause film rupture and dewetting. Again, the limit $\chi \to 0$ implies large deformation, and indeed the deformation is large compared to the film thickness that links the drops (in case of wetting fluids). But the actual size of the drops is expected to be small, so that the region $h_{\max} \to \infty$ is never approached. Evidently, for this drop-formation process surface tension must be large as we have already assumed.

We notice here that from the definition of δ in (25*c*) we can obtain a lower bound on the rate at which this parameter tends to zero. Indeed, $\delta \sim (We\, Re)^{1/2}/Ma^{3/2}$ which with

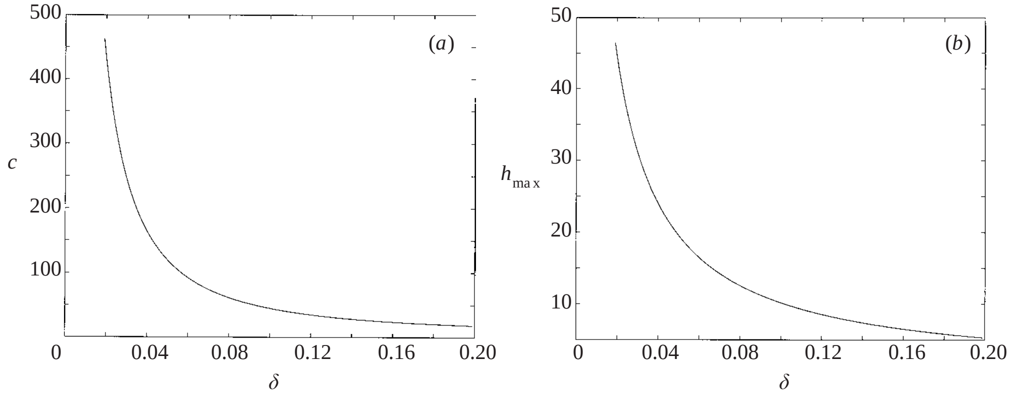

FIGURE 13. (a) Speed, c, and (b) maximum amplitude, $h_{\max}$, of the solitary pulses in figure 12 as a function of δ, in the region $\delta \ll 1$.

$We\,Re \sim \epsilon^{-2}$ yields $\delta \sim \epsilon^{-1}/Ma^{3/2}$. For $\delta \ll 1$, $Ma \gg \epsilon^{-2/3}$. For the derivation of our IBL approximation, $\epsilon \ll Ma \ll 1/\epsilon$ (see Kalliadasis *et al.* 1993). Hence, $\epsilon^{-2/3} \ll Ma \ll \epsilon^{-1}$, which gives a tighter lower bound on Ma. At the same time, $Ma \ll 1/\epsilon$, which gives $\epsilon^{-1}/Ma^{3/2} \gg \epsilon^{1/2}$ or $\delta \gg \epsilon^{1/2}$. Hence, δ can approach zero but at a rate slower than $\epsilon^{1/2}$.

Figure 13 shows $c = c(\delta)$ and $h_{\max} = h_{\max}(\delta)$. Both c and $h_{\max}$ blow up to infinity as $\delta \to 0$. Note that we also performed the computations for c and $h_{\max}$ in figure 13 by including the term $-\cot\theta h^3 h_x$ in (24). Our numerical results indicate that this term is important only in the two thin-film regions at the front and back of the large-amplitude solitary hump in figure 12 but it does not affect the hump itself. Hence, in the limit of small film thicknesses, the hydrostatic head in the direction perpendicular to the wall and inertial forces as well as heat transfer conditions on the free surface ($Bi \to 0$) are not important. The only important forces are 'friction' (associated with the mean flow induced by gravity), Marangoni and capillary forces. As a consequence, the bifurcation diagrams for c and $h_{\max}$ as a function of δ in figure 13 are independent of the inclination angle. This then implies that the bifurcation diagrams in the figure are universal for all θ, Re, Ma and γ.

The above observations indicate that the situation here is similar to the problem studied by Kalliadasis & Chang (1994) where the solitary wave speed is a monotonically increasing function of $(Re\,We/3)^{2/3}/R^2$ and blows up to infinity. For the fibre problem, the matched asymptotic analysis carried out by these authors for infinitely large homoclinic orbits demonstrated that the speed of the solitary waves blows up to infinity as $(Re\,We/3)^{2/3}/R^2 \to 1.413$ from below. In our case, however, there is no critical value for δ and solitary waves exist for all δ. An approach similar to Kalliadasis & Chang's for $c \to \infty$ is beyond the scope of the present study. Nevertheless, preliminary analysis of (32) as $\delta \to 0$ indicates that the solitary structures in figure 12 consist of an 'outer' region obtained by balancing the axial curvature $h^3 h_{\xi\xi\xi}$ with the Marangoni term $h^2 h_\xi$ and a Bretherton-type 'inner' region (Bretherton 1961), $h^3 h_{\xi\xi\xi} \sim \delta c(h-1)$. The analysis also indicates that, even though in figure 12 the maximum amplitude blows up to infinity faster than the width of the solitary waves, in terms of the original variables h and x (recall that we have rescaled x using ϕ in (25a)) the amplitude blows up to infinity slower than the width without violating the long-wave approximation.

Finally, for the problem of a thin film coating a vertical fibre, Chang & Demekhin (1999) demonstrated that the solitary pulses on the surface of the film can grow by an order of magnitude to form localized drops much larger in dimension than the film thickness away from the pulses. These authors also found that the drop formation process is mainly driven by a mechanism in the form of an ever-growing solitary pulse which leaves behind a trailing film thinner than the one it advances into. Moreover, the growing solitary pulse not only accumulates liquid from the film but also captures smaller (and therefore slower) pulses in a series of coalescence cascades. It is this coalescence cascade by a trailing solitary pulse that eventually leads to drop formation. The similarity between our solitary wave solution branch and the solution branch for the fibre problem indicates a similar scenario for our Marangoni problem.

6. Summary

We have considered the long-wave instabilities on the surface of a thin film falling down a uniformly heated wall in the region of small to moderate Reynolds numbers. The flow was modelled using the IBL approximation of the Navier–Stokes/energy equations and free-surface boundary conditions. In two-dimensions, IBL results in a system of three partial differential equations for the evolution of the local film thickess, flow rate and free-surface temperature distribution in time and space.

We analysed the linear stability of the flat-film solution with respect to two-dimensional and three-dimensional disturbances and demonstrated that by increasing either the inclination angle or the Marangoni number, the instability region (for the downstream propagating mode) becomes larger. We then focused on two-dimensional disturbances. For such disturbances we obtained two instability regions in the (χ, α)-plane associated with two different instability mechanisms for large and small χ respectively. For large χ (large film thicknesses, small deformation) inertia forces dominate Marangoni forces, while for small χ (small film thicknesses, large deformation) Marangoni forces dominate inertia. These two regions merge into a single instability region at zero wavenumber for sufficiently large M.

Our linear stability analysis shows the existence of three modes of instability: two surface modes propagating downstream and upstream respectively and a Marangoni mode. The only unstable mode is the downstream propagating surface mode. This is the usual hydrodynamic mode of instability for a falling liquid film. Its growth rate is found to be large and hence the thermocapillary effects act so as to amplify the hydrodynamic mode.

We then considered reduced models for the evolution of the free surface. We demonstrated that depending on the order of magnitude of the different parameters and on the way the neutral wavenumber approaches zero, in the weakly nonlinear stage of the instability we obtain either the KS or Kawahara's equation. In the limit $\chi \to 0$, the IBL approximation reduces to a single nonlinear equation for the film thickness. This equation contains only one parameter δ, suggesting a universal behaviour for the free surface in this limit. Finally, we examined the single-hump solitary wave solutions of IBL (with and without a slaved temperature field), Joo *et al.* equation and the model equation for $\chi \to 0$. In all cases, the IBL approximation with and without a slaved interface temperature give quite similar results for the free surface. However, the two approaches give different temperature distributions for the free surface with the difference between the two increasing as χ increases.

The solitary wave solution branch for the Joo *et al.* equation is in agreement with the one obtained from IBL up to an $O(1)$ value of χ at which the Joo *et al.* branch shows multiplicity and limit points above which solitary waves do not exist. On the other hand, the solitary wave solution branch of IBL does not exhibit any limit points/branch multiplicity. An important feature of the solution branch obtained from both the Joo *et al.* equation and IBL is that as $\chi \to 0$ (in this limit the two models are identical) both speed and solitary wave amplitude approach infinity, while for large values of χ, both speed and amplitude asymptote at a value which is independent of M. In the limit $\chi \to 0$, the solitary wave solution branch of the model equation with the single parameter δ approaches infinity as $\delta \to 0$. This, however, is not a true singularity formation, as forces of non-hydrodynamic origin, namely van der Waals forces not included here, become increasingly important in the region of very thin films and will arrest this blow-up behaviour.

Finally, there are are a number of arising questions from the analysis presented here. For example, it would be interesting to undertake a detailed comparison of the linear stability properties of our IBL approximation with the full Navier–Stokes/energy equations. Preliminary calculations indicate that IBL, despite the discrepancy for the critical conditions, predicts very well quantities like maximum growth wavenumbers and maximum growth wavelengths even for large Reynolds numbers. Although these preliminary comparisons for the linear stability properties of our IBL approximation with the full Navier–Stokes/energy equations are encouraging, our modelling can still be improved as we stated in § 3 in order to correctly predict the threshold of the instability close to the zero wavenumber limit and extend IBL to the region of large Reynolds numbers. In the absence of Marangoni effects this has been achieved using refined polynomial expansions and weighted residual techniques (Ruyer-Quil & Manneville 2002). Moreover, these authors took into account the second-order viscous terms which have been neglected in the present study. Indeed, these terms play an important role for the dispersion of the waves for larger Reynolds numbers. Therefore, a more refined modelling of the thermocapillary flow taking into account the second-order diffusive terms of the Navier–Stokes/energy equations and using high-order weighted residual techniques will follow (Ruyer-Quil *et al.* 2003).

At the nonlinear regime of the instability there are a number of problems to be addressed, for example, construction of the stationary waves, periodic and multi-hump solitary waves of our IBL approximation, and the stability of these waves with respect to two-dimensional and three-dimensional perturbations. In addition, of particular interest would be time-dependent computations, especially in the region of small χ, and a matched asymptotic analysis for $\delta \to 0$ to construct the infinitely large solitary waves in this limit. All these issues will be addressed in a separate study.

We are grateful to B. Scheid and Professor R. Kh. Zeytounian for fruitful discussions on thermocapillary effects and to Professor H.-C. Chang for numerous stimulating discussions on falling film dynamics. S.K. and E.A.D. thank the Instituto Pluridisciplinar for hospitality and acknowledge finanical support from EPSRC, through a Visiting Fellowship, grant no. GR/R61772/01 and the Spanish Ministry of Science and Technology under grant PB-96-599. Finally, we thank an anonymous referee for useful comments and suggestions.

REFERENCES

Alekseenko, S. V., Nakoryakov, V. E. & Pokusaev, B. G. 1994 *Wave Flow of Liquid Films*. Begel House.

Bankoff, S. G. 1994 Significant questions in thin liquid film heat transfer. *Trans. ASME J. Heat Transfer* **116**, 10–16.

Benney, B. J. 1966 Long waves in liquid films. *J. Math. Phys.* **45**, 150–155.

BRETHERTON, F. P. 1961 The motion of long bubbles in tubes. *J. Fluid Mech.* **10**, 166–188.

BUNOV, A. V., DEMEKHIN, E. A. & SHKADOV, V. YA 1984 On the non-uniqueness of nonlinear wave solitons in a viscous lauer. *Prikl. Matem. Mekhan.* **48**, 691–696.

BURELBACH, J. B., BANKOFF, S. G. & DAVIS, S. H. 1988 Nonlinear stability of evaporating/condensing liquid films. *J. Fluid Mech.* **195**, 463–494.

CHANG, H.-C. 1994 Wave evolution on a falling film. *Annu. Rev. Fluid Mech.* **26**, 103–136.

CHANG, H.-C. & DEMEKHIN, E. A. 1999 Mechanism for drop formation on a coated vertical fibre. *J. Fluid Mech.* **380**, 233–255.

CHANG, H.-C. & DEMEKHIN, E. A. 2002 *Complex Wave Dynamics on Thin Films.* Elsevier.

CHANG, H.-C., DEMEKHIN, E. A. & KALAIDIN, E. 1998 Generation and suppression of radiation by solitary pulses. *SIAM J. Appl. Maths* **58** 1246–1277.

CHANG, H.-C., DEMEKHIN, E. A. & KOPELEVICH, D. I. 1993*a* Laminarizing effects of dispersion in an active-dissipative nonlinear medium. *Physica* D **63**, 299–320.

CHANG, H.-C., DEMEKHIN, E. A. & KOPELEVICH, D. I. 1993*b* Nonlinear evolution of waves on a vertically falling film. *J. Fluid Mech.* **250**, 433–480.

CHANG, H.-C., DEMEKHIN, E. A. & KOPELEVICH, D. I. 1995 Stability of a solitary pulse against wave packet disturbances in an active medium. *Phys. Rev. Lett.* **75**, 1747–1750.

CHRISTOV, C. I. & VELARDE, M. G. 1995 Dissipative solitons. *Physica* D **86**, 323–347.

DEMEKHIN, E. A., DEMEKHIN, I. A. & SHKADOV, V. YA 1983 Solitons in flowing layer of a viscous fluid. *Izv. Akad. Nauk SSSR, Mekh. Zhidk Gaza* **4**, 9–16.

DEMEKHIN, E. A. & KAPLAN, M. A. 1989 Construction of exact numerical solutions of the stationary traveling type for viscous thin films. *Izv. Akad. Nauk SSSR, Mekh. Zhidk Gaza* **3**, 23–41.

DEMEKHIN, E. A., KAPLAN, M. A. & SHKADOV, V. YA 1987 Mathematical models of the theory of viscous liquid films. *Izv. Akad. Nauk SSSR, Mekh. Zhidk Gaza* **6**, 73–81.

DEMEKHIN, E. A. & SHKADOV, V. YA. 1984 Three-dimensional waves in a liquid flowing down a wall. *Izv. Akad. Nauk SSSR, Mekh. Zhidk Gaza* **5**, 21–27.

GESHEV, P. I. & EZDIN, B. S. 1985 Calculation of velocity profiles and wave form in falling liquid films. In *Hydrodynamics and Heat-Mass Transfer of Free-Surface Flows*, pp. 49–58. Institute of ThermoPhysics, Siberian Branch of the USSR Academy of Sciences, Novosibirsk (In Russian).

GOTTLIEB, D. & ORSZAG, S. A. 1977 *Numerical Analysis of Spectral Methods: Theory and Applications.* SIAM.

GOUSSIS, D. A. & KELLY, R. E. 1990 On the thermocapillary instabilities in a liquid layer heated from below. *Intl J. Heat Mass Transfer* **33**, 2237–2245.

GOUSSIS, D. A. & KELLY, R. E. 1991 Surface wave and thermocapillary instabilities in a liquid film flow. *J. Fluid Mech.* **223**, 25–45.

JOO, S. W., DAVIS, S. H. & BANKOFF, S. G. 1991 Long-wave instabilities of heated falling films: two-dimensional theory of uniform layers. *J. Fluid Mech.* **230**, 117–146.

KABOV, O. A. 1998 Formation of regular structures in a falling liquid film upon local heating. *Thermophys. Aeromech.* **5**, 547–551.

KALLIADASIS, S. & CHANG, H.-C. 1994 Drop formation during coating of vertical fibres. *J. Fluid Mech.* **261**, 135–168.

KALLIADASIS, S., KIYASHKO, A. & DEMEKHIN, E. A. 2003 Marangoni instability of a thin liquid film heated from below by a local heat source. *J. Fluid Mech.* **475**, 377–408.

KAWAHARA, T. 1983 Formation of saturated solitons in a nonlinear dispersive system with instability and dissipation. *Phys. Rev. Lett.* **51**, 381–383.

KAWAHARA, T. & TOH, S. 1988 Pulse interactions in an unstable dissipative-dispersive nonlinear system. *Phys. Fluids* **31**, 2103–2111.

KLIAKHANDLER, I. L., PORUBOV A. V. & VELARDE M. G. 2000 Localized fine-amplitude disturbances and selection of solitary waves. *Phys. Rev.* E **62**, 4959–4962.

KRISHNAMOORTHY, S., RAMASWAMY, B. & JOO, S. W. 1995 Spontaneous rupture of thin liquid films due to thermocapillarity: A full-scale direct numerical simulation. *Phys. Fluids* **7**, 2291–2293.

LIN, S. P. 1974 Finite amplitude side-band stability of a viscous film. *J. Fluid Mech.* **63**, 417–429.

NEKORKIN, V. I. & VELARDE, M. G. 1994 Solitary waves, soliton bound states and chaos in a dissipative Korteweg-de Vries equation. *Intl J. Bifurcat. Chaos* **5**, 1135–1146.

NEPOMNYASHCHY, A. A. 1974 Stability of wave regimes in a film flowing down an inclined plane. *Izv. Akad. Nauk SSSR, Mekh. Zhidk Gaza* **3**, 28–34.

Nepomnyashchy, A. A., Velarde, M. G. & Colinet, P. 2002 *Interfacial Phenomena and Convection*. Chapman & Hall.

Oron, A. 1999 Nonlinear dynamics of thin evaporating liquid films subject to internal heat generation. In *Fluid Dynamics at Interfaces* (ed. W. Shyy & R. Narayanan), Cambridge University Press.

Oron, A., Davis, S. H. & Bankoff, S. G. 1997 Long-scale evolution of thin liquid films. *Rev. Mod. Phys.* **69**, 931–980.

Oron, A. & Peles, Y. 1998 Stabilization of thin liquid films by internal heat generation. *Phys. Fluids* **10**, 537–539.

Pumir, A., Manneville, P. & Pomeau, Y. 1983 On solitary waves running down an inclined plane. *J. Fluid Mech.* **135**, 27–50.

Ramaswamy, B., Chippada, S. & Joo, S. W. 1996 A full-scale numerical study of interfacial instabilities in thin film flows. *J. Fluid Mech.* **325**, 163–194.

Ramaswamy, B., Krishnamourthy, S. & JOO, S. W. 1997 Three-dimensional simulation of instabilities and rivulet formation in heated falling films. *J. Comput. Phys.* **131**, 70–88.

Reid, R. C., Prausnitz, J. M. & Sherwood, T. K. 1977 *The Properties of Gases and Liquids*. McGraw-Hill.

Rosenau, P., Oron, A. & Hyman, J. M. 1992 Bounded and unbounded patterns of the Benney equation. *Phys. Fluids* A **4**, 1102–1104.

Ruyer-Quil, C., Kalliadasis, S., Zeytounian, R. Kh. & Velarde, M. G. 2003 Thermo-capillary long waves in a liquid film flow (in preparation).

Ruyer-Quil, C. & Manneville, P. 1998 Modeling film flows down inclined planes. *Eur. Phys. J.* B **6**, 277–292.

Ruyer-Quil, C. & Manneville, P. 2000 Improved modeling of flows down inclined planes. *Eur. Phys. J.* B **15**, 357–369.

Ruyer-Quil, C. & Manneville, P. 2002 Further accuracy and convergence results on the modeling of flows down inclined planes by weighted-residual approximations. *Phys. Fluids* **14**, 170–183.

Salamon, T. R., Armstrong, R. C. & Brown, R. A. 1993 Traveling waves on vertical films: Numerical analysis using the finite element method. *Phys. Fluids* **6**, 2202–2220.

Scheid, B., Oron, A., Colinet, P., Thiele, U. & Legros, J. C. 2002 Nonlinear evolution of non-uniformly heated falling liquid films. *Phys. Fluids* **14**, 4130–4151.

Shkadov, V. Ya 1967 Wave modes in the flow of thin layer of a viscous liquid under the action of gravity. *Izv. Akad. Nauk SSSR, Mekh. Zhidk Gaza* **1**, 43–50.

Shkadov, V. Ya 1968 Theory of wave flow of a thin layer of a viscous liquid. *Izv. Akad. Nauk SSSR, Mekh. Zhidk Gaza* **2**, 20–25.

Shkadov, V. Ya 1973 *Some Methods and Problems of the Theory of Hydrodynamic Stability*. Moscow: Izd. MGU (in Russian).

Smith, M. K. & Davis, S. H. 1983*a* Instabilities of dynamic thermocapillary liquid layers. Part 1. Convective instabilities. *J. Fluid Mech.* **132**, 119–144.

Smith, M. K. & Davis, S. H. 1983*b* Instabilities of dynamic thermocapillary liquid layers. Part 2. Surface-wave instabilities. *J. Fluid Mech.* **132**, 145–162.

Whitham, G. B. 1973 *Linear and Nonlinear Waves*. Wiley.

Zeytounian, R. Kh. 1998 The Bénard-Marangoni thermocapillary-instability problem. *Physics Uspekhi* **41**, 241–267.